

Bimodality of Lavas in the Teide–Pico Viejo Succession in Tenerife—the Role of Crustal Melting in the Origin of Recent Phonolites

SEBASTIAN WIESMAIER^{1,2,3*}, VALENTIN R. TROLL^{3,4},
JUAN CARLOS CARRACEDO³, ROBERT M. ELLAM⁵,
ILYA BINDEMAN⁶ AND JOHN A. WOLFF⁷

¹TRINITY COLLEGE DUBLIN, 2 COLLEGE GREEN, DUBLIN 2, IRELAND

²DEPARTMENT OF EARTH AND ENVIRONMENTAL SCIENCES, LUDWIG-MAXIMILIANS-UNIVERSITÄT, THERESIENSTR. 41, 80333 MÜNCHEN, GERMANY

³DPTO. FISICA - GEOVOL, UNIVERSITY OF LAS PALMAS DE GRAN CANARIA, 35017 LAS PALMAS DE GRAN CANARIA, CANARY ISLANDS, SPAIN

⁴DEPARTMENT OF EARTH SCIENCES, CEMPEG, UPPSALA UNIVERSITY, VILLAVÄGEN 16, 75236 UPPSALA, SWEDEN

⁵SCOTTISH UNIVERSITIES ENVIRONMENTAL RESEARCH CENTRE (SUERC), RANKINE AVENUE, SCOTTISH ENTERPRISE TECHNOLOGY PARK, EAST KILBRIDE G75 0QF, UK

⁶DEPARTMENT OF GEOLOGICAL SCIENCES, 1272 UNIVERSITY OF OREGON, EUGENE, OR 97403, USA

⁷DEPARTMENT OF GEOLOGY, WASHINGTON STATE UNIVERSITY, PULLMAN, WA 99164-2812, USA

RECEIVED OCTOBER 6, 2011; ACCEPTED JULY 20, 2012
ADVANCE ACCESS PUBLICATION SEPTEMBER 27, 2012

In Tenerife, lavas of the recent Teide–Pico Viejo central complex show a marked bimodality in composition from initially mafic lavas (200–30 ka) to highly differentiated phonolites (30–0 ka). After this abrupt change, the bimodality of the lavas continued to manifest itself between the now felsic Teide–Pico Viejo central complex and the adjacent, but exclusively mafic, rift zones. Whole-rock trace element fingerprinting distinguishes three compositional groups (mafic, transitional, felsic). Groundmass Sr–Nd–Pb–O and feldspar $\delta^{18}\text{O}$ data demonstrate open-system behaviour for the petrogenesis of the Teide–Pico Viejo felsic lavas by high $^{87}\text{Sr}/^{86}\text{Sr}$ ratios of up to 0.7049, uniform $^{206}\text{Pb}/^{204}\text{Pb}$ (19.75–19.78), variable $^{207}\text{Pb}/^{204}\text{Pb}$ (15.53–15.62) and heterogeneous $\delta^{18}\text{O}$ values (5.43–6.80‰). However, ocean sediment contamination can be excluded because of the low $^{206}\text{Pb}/^{204}\text{Pb}$ ratios of North Atlantic sediments. Isotope mixing hyperbolae reproduce the entire Teide–Pico Viejo succession and require an assimilant of predominantly felsic composition. Unsystematic and heterogeneous variation of $\delta^{18}\text{O}$ in fresh and unaltered feldspars across the Teide–Pico Viejo succession indicates

magmatic addition of diverse $\delta^{18}\text{O}$ assimilants, altered near surface at high and low temperatures. The best fit for these requirements is provided by nepheline syenite that occurs as fresh or altered lithic blocks in voluminous pre-Teide ignimbrite deposits and is similarly heterogeneous in oxygen isotope composition. Nepheline syenite blocks are considered to represent deep remnants of associated earlier eruptions and were thus available for assimilation at depth. Rare earth element modelling indicates that nepheline syenite needs to be melted in bulk to form a suitable end-member composition. Using this assimilant, energy-constrained assimilation fractional crystallization (EC-AFC) modelling reproduces the bulk of the succession, which leads us to suggest that Teide–Pico Viejo petrogenesis is governed by assimilation and fractional crystallization. Both mixing hyperbolae and EC-AFC models indicate that assimilation is more pronounced for the more felsic lavas. The maximum assimilation is evident in the most strongly differentiated (and the most radiogenic in Sr) lava and computes to >97.8% of the assimilant. This most evolved eruption probably represents nepheline syenite bulk melts

*Corresponding author. Present address: Department of Earth and Environmental Sciences, Ludwig-Maximilians-Universität, Theresienstr. 41, 80333 München, Germany. E-mail: sebastian.wiesmaier@min.uni-muenchen.de

that formed spatially decoupled from juvenile material. This study therefore recognizes a wider variability of magmatic differentiation processes at Teide–Pico Viejo than previously thought.

KEY WORDS: *crustal melting; anatexis; Teide; phonolite; ocean island evolution; Daly gap*

INTRODUCTION

The origin of abundant felsic volcanism in oceanic islands has long been a matter of debate. In a setting devoid of large regional tectonic influences and, for most ocean islands, extensive sedimentary sequences, it has commonly been proposed that crystal fractionation must be the dominant mechanism of differentiation (e.g. Cann, 1968; Schmincke, 1969; Clague, 1978; Garcia *et al.*, 1986; Ablay *et al.*, 1998; Thompson *et al.*, 2001). This is at odds, however, with the frequently observed bimodality of the lava compositions (Chayes, 1963). Early investigations of the compositional bimodality of the volcanic products [the ‘Bunsen–Daly Gap’, after Bunsen (1851) and Daly (1925) and later expanded on by Barth *et al.* (1939)] were largely concerned with the discussion of whether or not a gap actually existed between mafic and felsic end-member compositions (e.g. Chayes, 1963; Baker, 1968; Cann, 1968). This manifested itself in an argument about potential sample bias and suggestions for more detailed geological work (Harris, 1963; Baker, 1968; Cann, 1968). With respect to ocean islands, Schmincke (1969) identified a Bunsen–Daly gap in Gran Canaria, as did Ridley (1970) for erupted compositions in Tenerife. Fuster (1968) suggested that a gap is present in Fuerteventura, La Gomera, El Hierro and Lanzarote eruptive rocks. The Bunsen–Daly gap was commonly argued to be a consequence of fractional crystallization (e.g. Cann, 1968; Schmincke, 1969; Clague, 1978; Garcia *et al.*, 1986; Thompson *et al.*, 2001), but potential influences of partial melting were also mentioned (Chayes, 1977).

In continental epeirogenic settings (i.e. an arguably tectonically more complex environment compared with ocean islands) strong bimodalities also exist in the compositions of the erupted material. For example, in the east African Gregory Rift Valley the eruption of Miocene flood basalts was rapidly followed by large-volume plateau phonolites (Baker *et al.*, 1971). Estimated ratios of felsic to mafic eruption volumes range between roughly 0.5 and 1.5 for epochs from Miocene to Holocene, showing an overabundance of felsic material compared with what is expected from pure fractional crystallization scenarios (Williams, 1972). The lack of intermediate composition lavas between basalts and phonolites was considered to have originated from partial melting of upper mantle by a reduction in pressure by crustal upheaval or, alternatively, from an upper mantle that is hotter and thus more

susceptible to partial melting (Williams, 1970). Hypotheses on the origin of Kenyan phonolites that invoked partial melting of upper mantle material were criticized by Lippard (1973). Because of the trace element patterns of these highly differentiated phonolites, it was argued that they could not have formed by simple partial melting of mantle lithologies.

Explanations for bimodality started to diversify considerably in the 1980s. Crystal fractionation models were modified to allow for large crystal loads that restrain convection and induce bimodality in the erupted compositions (e.g. Marsh, 1981; Brophy, 1991, and references therein). Bailey (1987) suggested an upper mantle origin of trachytic melts, whereas Bonnefoi *et al.* (1995) invoked a model of critical cooling dynamics to explain the observed compositional relationships. More recently, assimilation of country rock has gained renewed momentum in differentiation models for magmas erupted on oceanic islands and is increasingly recognized (e.g. Thirlwall *et al.*, 1997; Bohrson & Reid, 1998; Garcia *et al.*, 1998; O’Hara, 1998; Harris *et al.*, 2000; Troll & Schmincke, 2002).

In Tenerife, too, fractional crystallization was long considered the main differentiation mechanism for the formation of felsic magmas (Wolff, 1983; Wolff & Storey, 1984). Relatively recently, recycling (i.e. partial or bulk melting) of rocks from within the island has been suggested to contribute to the evolution of felsic magmas in Tenerife (Wolff & Palacz, 1989; Wolff *et al.*, 2000). Major and trace element correlations of the products of the Teide–Pico Viejo strato-volcano (the most recent succession in Tenerife, <200 ka) have been explored in great detail by Ablay *et al.* (1998), who combined these with geothermobarometry calculations and estimates of pre-eruptive volatile contents. This allowed two lineages to be identified at Pico Viejo and Pico Teide, with each edifice having a somewhat different plumbing system. This is manifested in slightly different emplacement depths for the respective phonolite magma chambers. However, their interpretation of the Teide–Pico Viejo magmatic differentiation is de facto a closed-system fractional crystallization model with minor additions of zeolite and hydrothermally altered material being proposed to selectively explain trace element variations. Additionally, they discerned two distinct parental magmas for Teide and Pico Viejo. Their interpretation does not, however, incorporate the concept of rift zones (Carracedo, 1994, 1996), and the lack of stratigraphic constraints has since been much improved by new radiometric dating (Carracedo *et al.*, 2007). Systematic studies of the isotopic composition of lavas from Teide–Pico Viejo, the ultimate test for open- versus closed-system processes, had not been attempted.

We therefore investigated the isotope characteristics of lavas of the recent Teide–Pico Viejo succession and associated rift zones (<200 ka). We combine our detailed

isotopic dataset with existing major and trace element compositional data (Rodríguez-Badiola *et al.*, 2006). Our data show that the Teide–Pico Viejo succession is compositionally bimodal as a result of the combined effects of assimilation and fractional crystallization. Considerable percentages of melted country rock may be involved in the generation of the most strongly differentiated phonolites.

GEOLOGICAL BACKGROUND AND SAMPLE SET

The Canary Islands

The Canary Islands are the surface expression of a 750 km long volcanic belt that is located off Morocco (Fig. 1; see Geldmacher *et al.*, 2011). The archipelago comprises a chain of seven major islands, the shield stages of which show an east to west age progression from 20 Ma to 1.5 Ma (e.g. Carracedo, 1999). This has been mainly ascribed to the surface expression of a stationary mantle plume or hotspot below the moving and rotating African plate (Hoernle & Schmincke, 1993; Carracedo, 1994, 1996, 1999; Geldmacher *et al.*, 2011), but has also been related to regional deformation related to the Moroccan Atlas mountain range (Anguita & Hernán, 2000). As part of the African plate, which shows relatively slow motion at $\sim 10 \text{ mm a}^{-1}$, compared with oceanic crust in the Pacific (Duncan, 1981; Morgan, 1983), the Canary Islands are located on Mesozoic tholeiitic oceanic crust (Klitgord & Schouten, 1986; Verhoef *et al.*, 1991; Roest *et al.*, 1992; Schmincke & Rihm, 1994; Hoernle, 1998; Schmincke *et al.*, 1998; Neumann *et al.*, 2000). North and NE of Gran Canaria, the $\sim 7 \text{ km}$ thick igneous oceanic crust is overlain by up to 4 km of sediments (Ye *et al.*, 1999). This crustal package may be compacted to about 3 km of sediment (layer 1) and 2–4 km of igneous material (layers 2 and 3) beneath Gran Canaria, with the Moho at $\sim 15 \text{ km}$ depth (Kraestel & Schmincke, 2002).

Geology of Tenerife

Tenerife is the fourth of the seven emergent islands in the Canary Island archipelago and is located between Gran Canaria (older) and La Gomera (younger) (Abdel-Monem *et al.*, 1971, 1972). Three overlapping shield volcanoes (Roque Del Conde, Teno and Anaga) constitute the subaerial foundation of Tenerife and formed between 11.9 and 4 Ma (Carracedo, 1979; Ancochea *et al.*, 1990; Thirlwall *et al.*, 2000; Guillou *et al.*, 2004; Paris *et al.*, 2005; Walter *et al.*, 2005). The shield volcanoes exhibit mainly mafic volcanism, but up-section they also contain trachytic and phonolitic dykes, plugs and lava flows (e.g. Walter *et al.*, 2005; Longpré *et al.*, 2009). Activity migrated from the early central shield, Roque Del Conde, to the later

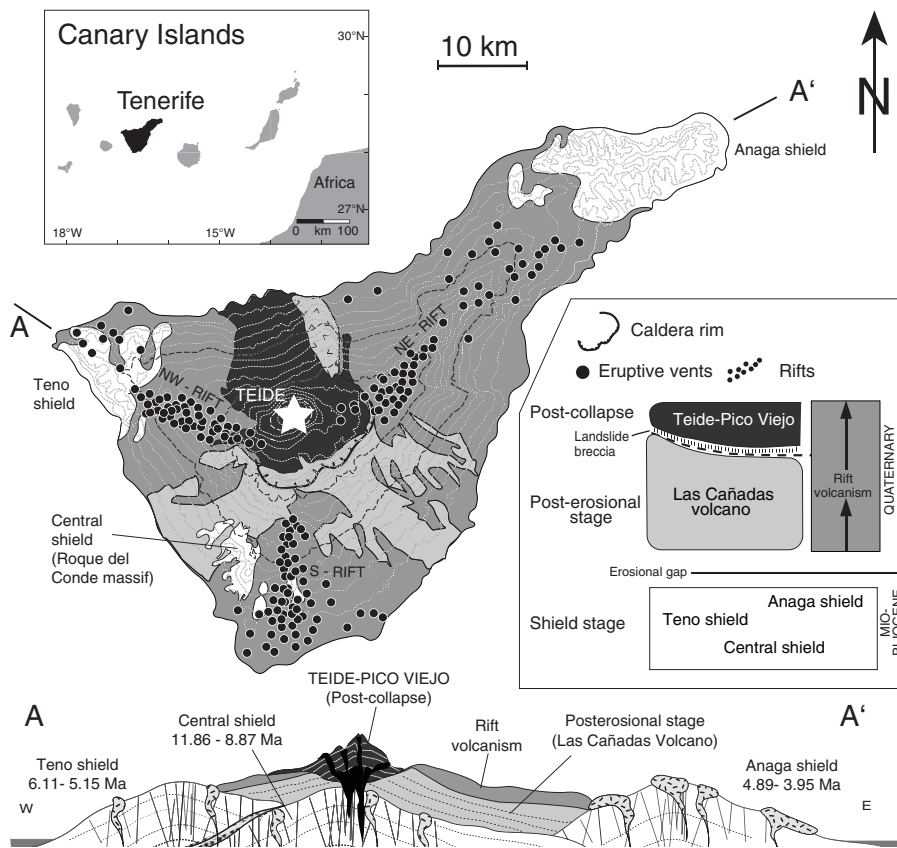
peripheral shields Teno and Anaga in the NW and NE, respectively (Guillou *et al.*, 2004).

The overall structure of Tenerife is controlled by a three-armed rift zone system. The three arms extend from the centre of the island to the south, NW and NE (Fig. 1). The NW and NE arms are currently active (Carracedo, 1994, 1996; Walter & Troll, 2003) and extend from beneath Teide–Pico Viejo volcano into Teno and Anaga (Carracedo *et al.*, 2007), but proto-rifts were already active as early as Miocene times (Carracedo *et al.*, 2010). The rifts are mainly characterized by mafic volcanism, with limited amounts of differentiated lavas that are restricted to nested intra-landslide eruptive rocks in the NE rift during the Pleistocene (Carracedo *et al.*, 2010). In recent times ($< 200 \text{ ka}$), rift eruptions have been exclusively mafic and originated from single or multiple, and often aligned, monogenetic cones.

After cessation of volcanic activity in the peripheral shields of Teno and Anaga, Tenerife's central part resumed eruptive activity at around 3.5 Ma to build the Las Cañadas volcano (Martí *et al.*, 1994; Ancochea *et al.*, 1999). This consists of a complex Lower Group formation (comprising multiple eruptive centres) and a three-cycle Upper Group. Each of these three Upper Group cycles broadly evolved from subordinate, primitive magmas to large-volume felsic eruptions. The second and third cycle of the Upper Group culminated in the caldera-forming ignimbrite formations of Granadilla ($\sim 570 \text{ ka}$) and Abrigo ($\sim 180 \text{ ka}$), respectively (e.g. Wolff, 1983; Martí *et al.*, 1994, 1997; Bryan *et al.*, 2000; Martí & Gudmundsson, 2000; Brown *et al.*, 2003; Brown & Branney, 2004; Edgar *et al.*, 2007). At around 200–180 ka, a giant landslide formed the Icod collapse scar (Watts & Masson, 1995; Carracedo, 1999; Carracedo *et al.*, 2007; Márquez *et al.*, 2008). However, pre-existing vertical collapse structures may have contributed to the lateral instability of Las Cañadas volcano (e.g. Martí *et al.*, 1994, 1997; Troll *et al.*, 2002). The Icod landslide unroofed the central Las Cañadas volcano (and the underlying rift zone triple-junction), initiating the construction of the Teide–Pico Viejo complex nested inside the Icod collapse embayment (Fig. 1; see Márquez *et al.*, 2008).

Initial eruptions at Teide–Pico Viejo were of mafic composition indistinguishable from the rift zone eruptions. However, between 30 and 20 ka, the Teide–Pico Viejo edifice and its flank vents began to erupt phonolite, which became the exclusive lava composition in the last 20 kyr (Carracedo *et al.*, 2007). These phonolite eruptions are two to three orders of magnitude larger than 'normal' rift zone basanite or tephrite eruptions (Carracedo *et al.*, 2008). Mafic activity continued in the adjacent rift zones with on average one eruption per century. In the boundary zone between the rift zones and the central complex, mixing of tephrite and phonolite magmas has been shown to occur

(a) Tenerife Geology



(b) Lavas Teide-Pico Viejo and rift zones (<200ka)

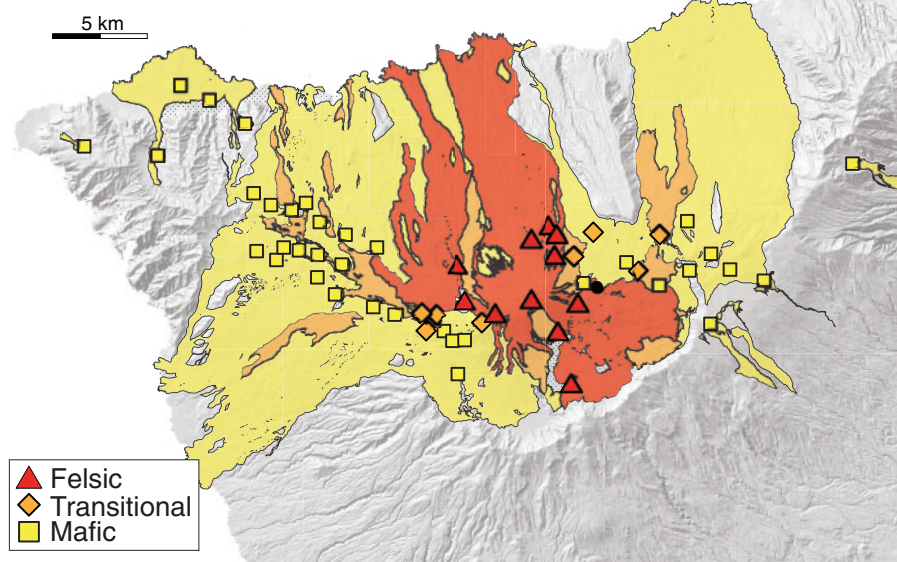


Fig. 1. (a) Simplified geological map of Tenerife (after Carracedo *et al.*, 2007). The distribution of monogenetic vents (black circles) that indicates the three rift zones to the south, NE and NW should be noted. (b) Distribution of eruption centres of the Teide–Pico Viejo succession in Tenerife. Triangles, felsic lavas; diamonds, transitional lavas; squares, mafic lavas. The black circle indicates Montaña de los Conejos, which was not included in our study because whole-rock data were not available. The clustering of felsic lavas around the central complex should be noted. The mafic lavas define the rift zones, but also occur in the older products of the central complex, with the transitional lavas falling into the geographical and chemical transition between the mafic and felsic lavas.

(Araña *et al.*, 1994; Wiesmaier *et al.*, 2011). Because of the similarity of early Teide and rift zone eruptions, the rift zones and central complex may be considered part of the same overall system, including distal rift zone eruptions that are not interbedded with deposits erupted from the central complex. Therefore, the central Teide–Pico Viejo complex inside the Las Cañadas Caldera and the coeval eruptions in the NW and NE rift zones are termed the ‘Teide–Pico Viejo succession’ hereafter.

Previous studies and sample set

The present study focuses on the Sr–Nd–Pb isotope compositions of the Teide–Pico Viejo lavas on Tenerife. Previous publications have provided detailed age and stratigraphic constraints and a whole-rock major and trace element dataset for 98 representative samples (Rodríguez-Badiola *et al.*, 2006; Carracedo *et al.*, 2007). From this sample set, our samples were selected to cover 58 of the 64 known eruptions within the succession (Table 1), allowing for the fact that some eruptions comprise multiple phases. Moreover, six of the currently known 64 eruptions were discovered only after sampling for this study was completed and, hence, are not included (Carracedo *et al.*, 2007).

The sample suite includes rift zone basanites and tephrites that are aphyric or contain olivine (ol) \pm clinopyroxene (cpx) \pm plagioclase (plag phenocrysts). Phonotephrites and tephriphonolites are from lava flows either grouped around the wider perimeter or that form part of the central Teide–Pico Viejo complex. These rocks either are aphyric or contain cpx \pm plag \pm amphibole (amp) \pm magnetite and/or ilmenite (mt/il phenocrysts). Phonolites are geographically restricted to the central complex and radial vents of this edifice and contain alkali feldspar (afp) \pm cpx \pm amp \pm biotite (bt) \pm mt/il phenocrysts.

Classification of samples

In a total alkali vs SiO₂ (TAS) diagram (Le Bas *et al.*, 1986), rocks from the Teide–Pico Viejo succession define an alkaline trend from basanite to phonolite with some excursions into the trachytic series (Fig. 2). The dataset comprises 97% of the known eruptions of the last 200 kyr, and includes only one sample per stratigraphic unit to avoid sample bias or over-representation.

The Teide–Pico Viejo lavas are categorized into three groups on the basis of their whole-rock trace element patterns. Parallel trace element patterns (i.e. trends that do not cross-cut each other) indicate related combinations of trace element ratios (see Lippard, 1973). Relative enrichments or depletions in the elements Pb, Ba and Sr are characteristic of each of the three groups of mafic, transitional and felsic lavas (Fig. 3). As a first approximation, lavas of each group are assumed to have experienced a comparable magmatic history. Throughout the following text, the terms mafic, transitional and felsic exclusively refer to the trace element classification adopted here.

The mafic lavas comprise all the basanites and tephrites from the rift zones, one foidite, one basaltic trachyandesite and several intra-caldera and Teide–Pico Viejo phonotephrites and trachybasalts. They exhibit a negative Pb anomaly relative to the neighbouring elements in their multi-element patterns (Fig. 3). The mafic lavas are the most abundant in this study ($n = 40$).

The transitional samples range from trachyandesites to trachyte and from tephriphonolites to phonolites. These samples show positive Pb anomalies, negative Sr anomalies and small positive to weak negative Ba anomalies (Fig. 3). The transitional lavas ($n = 10$) erupted from the margins of Teide–Pico Viejo complex or vents inside the Las Cañadas Caldera and they define the compositional boundary between the rift zones and central complex.

The felsic lava group comprises phonolites that erupted from Teide–Pico Viejo or the flank vents of the volcano. These ($n = 12$) include Montaña Blanca, Roques Blancos and the last eruption from Teide’s central vent (Lavas Negras, 1150 ± 140 a BP, Carracedo *et al.*, 2007). The felsic group is defined by strongly negative anomalies in both Sr and Ba, with Sr_n always being below 10 (normalized to primitive mantle) (Fig. 3).

In the TAS diagram (Fig. 2), the mafic lavas show a continuous differentiation trend towards transitional compositions, with a narrow range in alkali variability. Transitional lavas have much more scattered compositions ranging from tephriphonolite to phonolite and trachyte. The felsic lavas define a separate and steep trend at an angle to the main differentiation trend defined collectively by all three groups. Geographically, the vents of the three compositional groups display a concentric arrangement around the central Teide–Pico Viejo complex (see Fig. 1b).

The total volume of the Teide–Pico Viejo complex is estimated to be 160 km³, divided into 62 km³ of initial filling of the collapse embayment (mafic), 70 km³ for the old Teide edifice (mafic, transitional), 15 km³ for Pico Viejo volcano (mafic and transitional), 6.5 km³ for Teide satellite vents (felsic) and 0.7 km³ for the final construction of the Teide stratocone (felsic). Rift zone estimates range from around 32 and 9 km³ for the NW and NE rift zones respectively. The distinction between mafic, transitional and felsic lavas is poorly defined in these estimates, owing to partial or complete burial of units older than 15 ka. In contrast, it is possible to constrain the volume of the more recent eruptions at Teide–Pico Viejo (<15 ka) on an individual basis (Fig. 4; Carracedo *et al.*, 2008). Mafic lavas erupt more frequently but with small volumes, whereas felsic lavas erupt less frequently but with large volumes. Transitional lavas have declined in frequency over the last 15 kyr and are lower than the mafic lavas in their cumulated volume. The felsic lavas, in turn, dominate volumetrically over the last 15 kyr. Combined with the large volumes of mafic lavas during the initial filling of the

Table 1: Sampled eruptions from Teide–Pico Viejo succession and types of analyses performed

Eruption	Phase	Samples	Analyses	Composition
Abejera Alta		ABA-21, ABA-22, ABA-36*	Pb	Evolved
Abejera Baja		ABB-19, ABB-20	Pb	Evolved
Montaña Abeque		ABQ-47*	Sr	Primitive
Volcán de Arafo		ARA-01*	Pb, Sr, Nd	Primitive
Montaña Arenas Negras		ARE-13	Pb, Sr, Nd	Primitive
Montaña del Banco		BAN-53	Pb, Sr, Nd	Primitive
Montaña Bilma		BIL-34*, BIL-36	Pb, Sr, Nd	Primitive
El Boquerón		BOQ-13, BOQ-14	Pb	Evolved
Montaña Botija		BOT-28*	Pb, Sr, Nd	Primitive
Montaña Cascajo	Phase 1	CA1-21, CA1-23*, CA1-75	Pb, Sr, Nd,	Primitive
			O	
	Phase 2	CA2-20*	Pb, Sr, Nd	Primitive
	Phase 3	CA3-22, CA3-24*	Pb, Sr, Nd	Primitive
Pico Cabras		CAB-27	Pb, Sr, Nd	Evolved
Volcán de Boca Cangrejo		CAN-05, CAN-06*	Pb, Sr, Nd	Primitive
Chahorra		CHA-03*	Pb, Sr, Nd	Primitive
Chinyero		CHI-01*	Pb, Sr, Nd	Primitive
Volcan El Ciego		CIE-18, CIE-19*	Pb, Sr	Transitional
Montaña de Chío		CIO-32, CIO-77, CIO-81, CIO-82, CIO-83	Pb, Sr, Nd,	Primitive
			O	
Montaña de Las Colmenas		COL-15*	Pb	Primitive
Montaña de Los Corrales		COR-04*, COR-05	Pb, Sr, Nd	Transitional
Montaña Cruz		CRU-39*	Pb, Sr, Nd	Primitive
Volcán Cuevas Negras		CUE-14*	Pb, Sr, Nd,	Primitive
			O	
Montaña de La Cruz		DLC-18*	Evolved	
Montaña Estrecho		EST-40*, EST-41	Pb, Sr, Nd	Primitive
Fasnia, Siete Fuentes		FAS-02*	Pb, Sr	Primitive
Montaña Garachico		GAR-04*	Pb, Sr	Primitive
Galería Rio de Guía (PV-EVO)		GRG-1300, GRG-2800, GRG-2850		
Montaña Guamasa		GUA-17	Pb, Sr	Primitive
Volcán Los Hornitos		HOR-17	Pb, Sr	Primitive
Montaña Juan Évora		JEV-03*	Pb, Sr	Primitive
Montaña Las Lajas		LAJ-23, LAJ-24*	O	Transitional
Las Lenguas		LEN-15*	Pb, Sr, O	Transitional
Montaña Majúa		MAJ-16, MAJ-17*	Pb, Sr, O	Evolved
Bocas de Doña María		MAR-31, MAR-37	Pb, Sr, O	Primitive
Montaña Blanca	Phase 1	MB1-34		Evolved
	Phase 3	MB3-11*		Evolved
	Phase 4	MB4-10*		Evolved
	Phase 5	MB5-04*, MB5-05	Pb	Evolved
	Phase 6	MB6-12*		Evolved
	Phase 7	MB7-08*	Pb, Sr	Evolved
	Phase 8	MB8-06, MB8-09*	Pb, Nd	Evolved
Montañetas Negras		MNE-33*	Pb, Sr	Primitive

(continued)

Table 1: Continued

Eruption	Phase	Samples	Analyses	Composition
Montaña Negra (Bco. de Vergara)		VER-32	Pb, Sr	Transitional
Montaña Mostaza		MOS-11*	Pb, Sr	Primitive
Montañas Negras		NEG-50, NEG-51	Pb, Sr, O	Primitive
Volcán del Palmar		PAL-56, PAL-57*	Pb, Sr	Primitive
Volcán Portillo	Lower	PO1-06*	Pb, Sr	Transitional
	Upper	PO2-07, PO2-09	Pb, Sr	Transitional
Pico Teide, Lavas Antiguos (Playa Sto. Domingo)		PT-ANT-16	Pb, Sr	Primitive
Pico Teide, Lavas Antiguos (Playa San Marcos)		PT-EAR-15	Pb	Primitive
Pico Teide, Intermediate Lavas		PT-INE-07, PT-INE-11, PT-INE-17	Pb, Sr, O	Transitional
Pico Teide, Lavas Negras		PT-LAE-02*, PT-LAE-03, PT-LAE-04, PT-LAE-05, PT-SUM-01	Pb, Sr, O	Evolved
Pico Viejo, Pa'hoehoe Lavas		PV-EAR-13, PV-EAR-15, PV-EAR-16, PV-EAR-17	Pb, Sr, O	Primitive
Pico Viejo, Evolved Lavas		PV-EVO-05*, PV-EVO-06, PV-EVO-07, PV-EVO-21, PV-EVO-28	Pb, Sr, O	Primitive
Pico Viejo, Intermediate Lavas		PV-INT-08, PV-INT-09, PV-INT-18, PV-INT-29	Pb, Sr, O	Primitive
Pico Viejo, Lavas De La Orotava		PV-LAT-01	Pb, Sr	Transitional
Pico Viejo, Phonolite I		PV-LAT-02, PV-LAT-03*, PV-LAT-04, PV-LAT-61, PV-LAT-66	O	Transitional
Cuevas del Ratón		RAT-44, RAT-84	Pb, Sr, O	Primitive
Roques Blancos		RBL-01, RBL-02*, RBL-03	Pb, Sr, O	Evolved
Montaña Reventada	Basanite	REV-87	Pb, Sr	Primitive
	Phonolite	REV-10, REV-64*, REV-71, REV-85	Pb, Sr	Transitional
	Enclaves	REV-09, REV-63*		Primitive
Montaña Samara		SAM-26, SAM-27	Pb, Sr	Primitive
Montaña de Los Silos		SIL-60	Pb, Sr	Primitive
Montaña de Taco		TAC-58	Pb	Primitive
Montaña de los Tomillos		TOM-14	Pb	Primitive
Montaña del Topo		TOP-55	Pb	Primitive
Volcán Tierra del Trigo		TRI-61	Pb, Sr	Primitive
Volcán Negro		VON-12, VON-13	Pb	Primitive

*Samples from the dataset of Rodríguez-Badiola *et al.* (2006).

Details on sample location, age, dating method and vent locations have been given by Carracedo *et al.* (2007). Types of analysis: Pb indicates Pb isotopes; Sr indicates $^{87}\text{Sr}/^{86}\text{Sr}$; Nd indicates $^{143}\text{Nd}/^{144}\text{Nd}$; O indicates $\delta^{18}\text{O}$. Composition column indicates the classification of the lava according to its trace element fingerprint. Some eruptions comprise multiple phases of close temporal relation. Eruptions and phases not represented in this study: Montaña Blanca Phase 2 (phonolite), *La Mancha Ruana (phonolite, between Teide and Pico Viejo), *Hoya del Abrunco (trachyte, below Abejera Baja and Pico Cabras), *PT-CALV (mafic phreatomagmatic eruption Teide- Pico Viejo), PV-PHR (phreatomagmatic eruption Pico Viejo), Los Gemelos (small phonolite eruption between Teide and Pico Viejo), *Montaña Liferfe (phonotephrite NW rift zone).

collapse scar, the transitional lavas are probably subordinate to both felsic and mafic lavas. The compositional bimodality of the lava flows is thus evident in both eruptive frequency and estimates of erupted volume.

METHODS

Isotopic analyses of groundmass samples

Wiesmaier (2010) performed microanalysis on feldspar phenocrysts, indicating the presence of abundant glomerocrysts

and disequilibrium phenocrysts in the Teide–Pico Viejo lavas. We therefore analysed groundmass separates from 61 samples for their Pb, Sr and Nd isotopic composition. Fresh groundmass represents the very last melt composition and is, when properly separated, completely unaffected by any masking effects from accumulation of phenocrysts or xenocrysts, thus allowing melt processes to be constrained more reliably. Apart from several duplicate analyses, only one sample per lava flow was analysed to avoid over-representation of any particular unit.

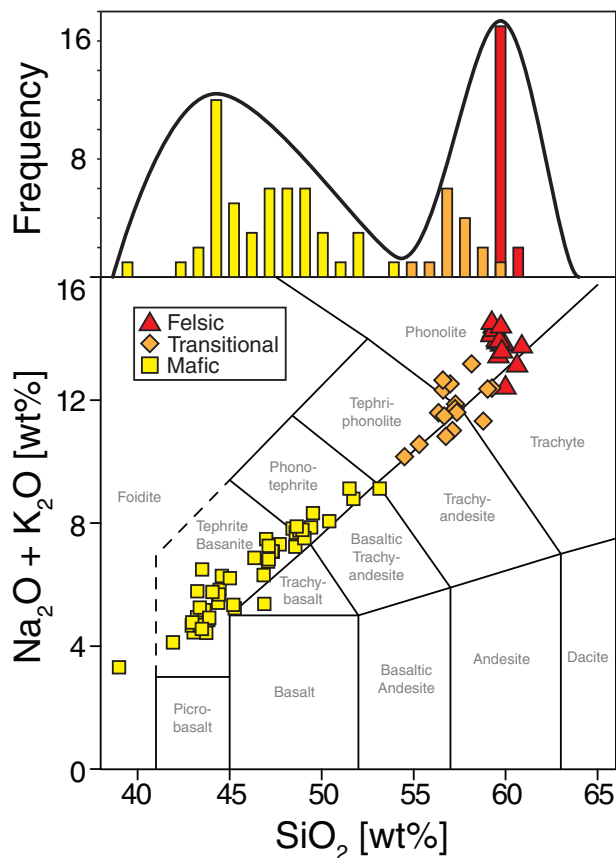


Fig. 2. Teide–Pico Viejo samples plotted in a total alkalis vs silica (TAS) diagram after Le Bas *et al.* (1986).

Samples were analysed for their $^{206}\text{Pb}/^{204}\text{Pb}$, $^{207}\text{Pb}/^{204}\text{Pb}$ and $^{208}\text{Pb}/^{204}\text{Pb}$, $^{87}\text{Sr}/^{86}\text{Sr}$ and $^{143}\text{Nd}/^{144}\text{Nd}$ ratios. Four of the 40 mafic lavas, two of the 10 transitional samples and one of the 11 felsic lavas were analysed in duplicate. Moreover, five sedimentary rocks of exhumed pre-island seafloor from Fuerteventura were analysed to represent potential end-members for the isotopic composition of non-magmatic rocks that may be trapped underneath or within the crust of the islands (e.g. Fúster *et al.*, 1968; Stillman *et al.*, 1975; Hobson *et al.*, 1998; Hansteen & Troll, 2003). Samples were freed from weathered surfaces and jaw-crushed. Chips were hand-picked under a stereomicroscope to exclude crystalline, weathered or xenolithic material. The chips were then ground by hand using an agate mortar and pestle. A total of 69 Pb–Pb, 53 Sr and 30 Nd isotope analyses of groundmass are reported here. Data for all three radiogenic isotope systems are reported with 2SD errors (Table 2).

All groundmass isotopic analyses, including the necessary clean laboratory procedures, were carried out at the Isotope Geosciences Unit of the Scottish Universities Environmental Research Centre (SUERC), East Kilbride,

UK. Samples for Pb, Sr and Nd were weighed and placed into PFA Teflon screw-top beakers (Saville[®]) and were then dissolved using ultra-pure reagents in an HF–HNO₃–HCl acid digestion. All samples were handled in a cleanbox located within a clean laboratory.

Pb–Pb analysis

The procedure for Pb analysis followed that of Ellam (2006). After digestion, the sample was put through columns made from ultraclean pipette tips and Eichrom Sr-Spec resin to separate Pb from other ions. Lead was eluted with 6 M HCl, after which the sample was conditioned with concentrated HNO₃ and finally diluted to 50 ppb in a mixture of 5% HNO₃ + 5 ppb Tl. The total procedure Pb blank was below 1 ng.

A Micromass IsoProbe multi-collector inductively coupled plasma mass spectrometry (MC-ICP-MS) system using a 50 $\mu\text{L min}^{-1}$ PFA nebulizer fitted to an Elemental Scientific[®] Apex nebulizer with an ACM desolvation unit was utilized for measurements of Pb isotopes. Beam intensities of ^{208}Pb ranged around 1 V (1×10^{-11} A), and analyses were conducted in five blocks of 20 ratios with 5 s integrations in static multi-collection mode. Samples were analysed by MC-ICP-MS with Tl-doping to account for Pb mass bias (Belshaw *et al.*, 1998; Rehkämper & Halliday, 1998; White *et al.*, 2000). An exponential law with a $^{205}\text{Tl}/^{203}\text{Tl}$ ratio of 2.3871 was chosen. Baselines were measured on-peak for 45 s in 5% HNO₃. During the course of a several hour analytical session, Pb memory build-up was accounted for by introducing a solution of 5% HNO₃–2% HF into the ICP-MS system for 2 min between sample runs. Uncorrected NIST SRM981 standard runs gave $^{206}\text{Pb}/^{204}\text{Pb} = 16.941 \pm 24$, $^{207}\text{Pb}/^{204}\text{Pb} = 15.501 \pm 22$ and $^{208}\text{Pb}/^{204}\text{Pb} = 36.721 \pm 58$ (all 2SD, $n = 15$).

Sr and Nd isotope measurements

Strontium was separated in 2.5 N HCl using Bio-Rad AG50W X8 200–400 mesh cation exchange resin. Neodymium was separated from the previously separated rare earth element (REE) concentrate in a mixture of acetic acid (CH₃COOH), methanol (CH₃OH) and nitric acid (HNO₃) using Bio-Rad AGIX8 200–400 mesh anion exchange resin. Total procedure blanks for Sr and Nd were less than 0.5 ng. Analysis was performed on a VG Sector 54-30 thermal ionization, multiple collector mass spectrometer.

Samples for Sr isotope analysis were loaded onto single Ta filaments. A ^{88}Sr intensity of 1 V (1×10^{-11} A) $\pm 10\%$ was maintained. The $^{87}\text{Sr}/^{86}\text{Sr}$ ratio was corrected for mass fractionation using $^{86}\text{Sr}/^{88}\text{Sr} = 0.1194$ and an exponential law. The mass spectrometer was operated in the peak-jumping mode with data collected as 15 blocks of 10 ratios. The NBS987 standard yielded a $^{87}\text{Sr}/^{86}\text{Sr}$ value of 0.710252 ± 26 (2SD, $n = 49$).

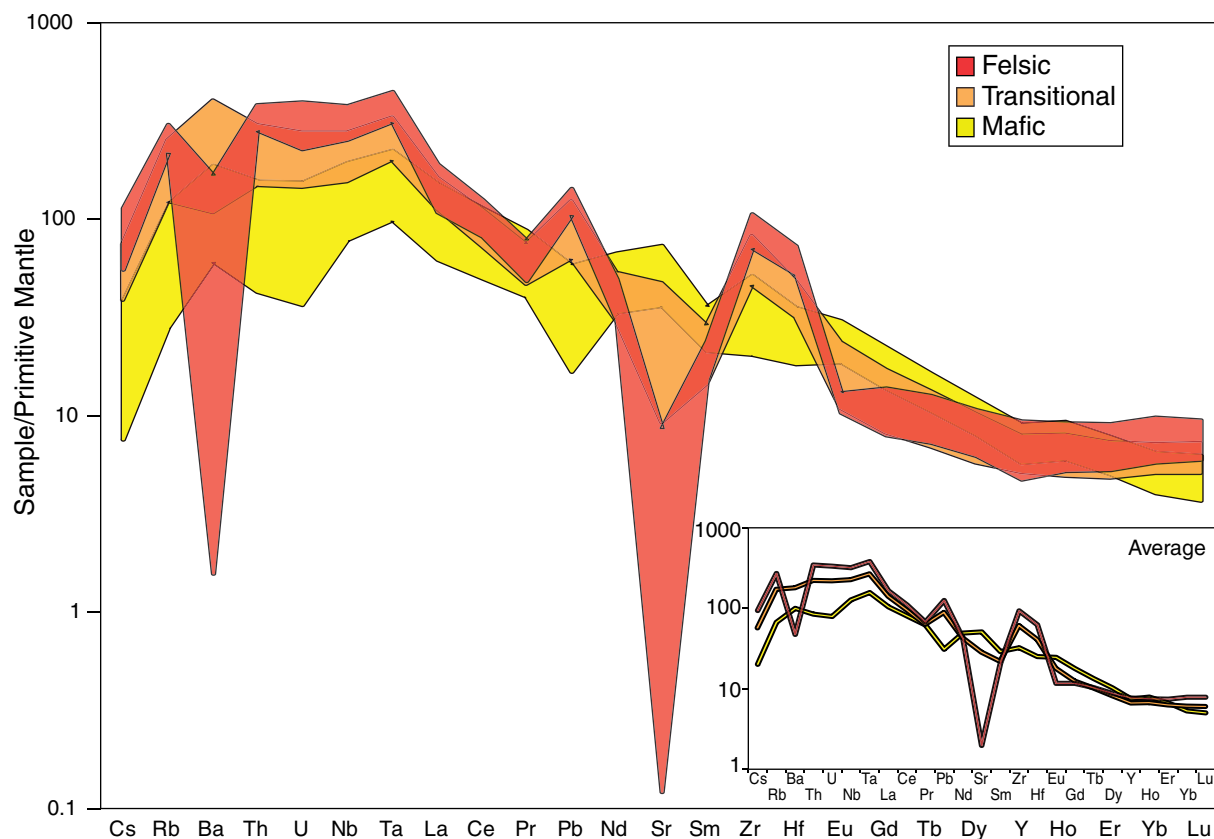


Fig. 3. Multi-element variation diagram for post-collapse lavas from Tenerife, normalized to the primitive mantle values of McDonough & Sun (1995). Inset shows averages of each group.

Samples for Nd isotope analysis were loaded onto triple Ta–Re–Ta filaments. $^{143}\text{Nd}/^{144}\text{Nd}$ ratios were measured with a ^{144}Nd beam of 1 V (1×10^{-11} A). Twelve blocks of 10 ratios were collected in peak jumping mode and corrected for mass fractionation using an exponential law and $^{146}\text{Nd}/^{144}\text{Nd} = 0.7219$. Repeat analyses of the internal laboratory standard (JM) yielded a $^{143}\text{Nd}/^{144}\text{Nd}$ ratio of 0.511517 ± 21 (2SD, $n = 25$).

Oxygen isotope analysis

Feldspar separates from 15 lava flows were analysed for their $\delta^{18}\text{O}$ composition. Six of these 15 units were also analysed for the $\delta^{18}\text{O}$ composition of their groundmass. Analyses were performed in the stable isotope laboratory at the University of Oregon (Bindeman, 2008). Plagioclase phenocrysts were analysed by laser fluorination to determine $\delta^{18}\text{O}$ values using 1–2 mg of unaltered phenocrysts (1–3 single crystals for each analysis). After laser extraction with a 35 W Newwave CO_2 laser in a BrF_5 atmosphere, each sample was purified from traces of fluorine gas by boiling mercury and converted to CO_2 . A yield of close to 95% CO_2 indicated limited reaction of the samples with BrF_5 at room temperature. The laser fluorination line was coupled to a Finnigan MAT 253 mass spectrometer and

normalized to garnet standard GMG = +5.75‰ values. Standards measured during the experiment runs were $+5.61 \pm 0.06\%$ (1SD; $n = 12$). Owing to daily variations, our standards were calibrated to the SMOW scale by adding between 0.10 and 0.23‰ to the measured values on the unknowns. Based on repeated analyses of standards, the maximum analytical uncertainties on $\delta^{18}\text{O}$ measurements are estimated at 0.1‰. The ‘melt’ values were calculated using the equation $\delta^{18}\text{O}_{\text{melt}} = \delta^{18}\text{O}_{\text{plag}} + [0.027 \times \text{SiO}_2 (\text{wt } \%) - 1.45]$, which models equilibrium mineral–melt fractionation (Bindeman *et al.*, 2004).

RESULTS

Isotope ratios in groundmass samples

Strontium isotope composition in groundmass samples

Analysis of the $^{87}\text{Sr}/^{86}\text{Sr}$ composition in the groundmass was carried out on 34 mafic, nine transitional and six felsic samples (plus four duplicate analyses) (Table 2). The data are reported with uncertainties of 2SD. Mafic and transitional lavas overlap considerably in $^{87}\text{Sr}/^{86}\text{Sr}$ [mafic: $0.703040 (\pm 21)$ to $0.703229 (\pm 18)$; transitional: $0.703094 (\pm 20)$ to $0.703332 (\pm 17)$], with only one transitional

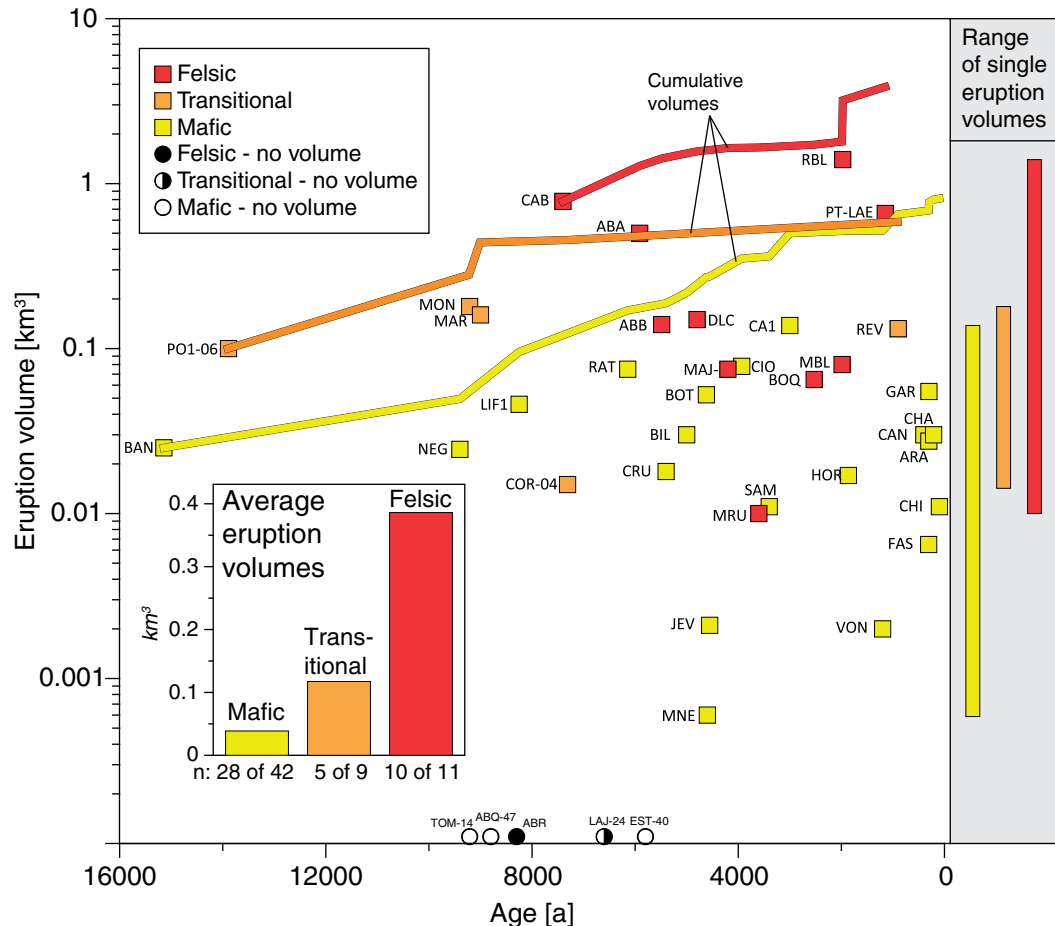


Fig. 4. Eruption volumes vs stratigraphic and radiometric ages of Teide–Pico Viejo lavas younger than 15 ka (data from Carracedo *et al.*, 2007, 2008).

sample outside the range of the mafic group. This sample, a phonolite from Montaña Reventada that is part of a composite eruption of basanite and phonolite, shows abundant mixing and mingling textures (Araña *et al.*, 1994; Wiesmaier *et al.*, 2011). In contrast, the felsic lavas yield $^{87}\text{Sr}/^{86}\text{Sr}$ of 0.703091 (± 2) to 0.704900 (± 6), significantly higher values than the mafic and the transitional lavas. Two Fuerteventura sediment samples yielded Sr isotope ratios of 0.703473 (± 21) and 0.707684 (± 21). The upper limits of Sr isotope range increase with increasing degree of differentiation (Table 2).

Neodymium isotope composition in groundmass samples

Analysis of $^{143}\text{Nd}/^{144}\text{Nd}$ was undertaken on groundmass separates from 20 mafic, four transitional and six felsic samples. Mafic lavas yield $^{143}\text{Nd}/^{144}\text{Nd}$ values of 0.519201–0.512991 (± 6 –45). Transitional samples are constrained to a smaller interval of $^{143}\text{Nd}/^{144}\text{Nd}$, ranging between 0.512916 and 0.512956, and felsic samples plot in an even tighter range of 0.512924–0.512950 (Table 2).

Pb–Pb composition of groundmass samples

A total of 69 samples were analysed for their $^{206}\text{Pb}/^{204}\text{Pb}$, $^{207}\text{Pb}/^{204}\text{Pb}$ and $^{208}\text{Pb}/^{204}\text{Pb}$ isotopic ratios. Among these samples were 61 lava flows, plus three duplicate analyses to test data reproducibility and five sediment samples from Fuerteventura. Grouped by their degree of differentiation, the lavas yielded the following ratios (reported with 2SD in parentheses; Table 2).

Mafic lavas: $^{206}\text{Pb}/^{204}\text{Pb}$ ratios range from 19.505 (± 22) to 19.814 (± 22), $^{207}\text{Pb}/^{204}\text{Pb}$ from 15.592 (± 22) to 15.646 (± 24) and $^{208}\text{Pb}/^{204}\text{Pb}$ from 39.449 (± 68) to 39.637 (± 68) ($n = 40$, plus two duplicates).

Transitional lavas: $^{206}\text{Pb}/^{204}\text{Pb}$ ratios range from 19.749 (± 26) to 19.774 (± 26), $^{207}\text{Pb}/^{204}\text{Pb}$ from 15.610 (± 24) to 15.634 (± 28) and $^{208}\text{Pb}/^{204}\text{Pb}$ from 39.554 (± 70) to 39.607 (± 80) ($n = 10$, plus one duplicate).

Felsic lavas: $^{206}\text{Pb}/^{204}\text{Pb}$ ratios range from 19.754 (± 28) to 19.782 (± 24), $^{207}\text{Pb}/^{204}\text{Pb}$ from 15.529 (± 22) to 15.617 (± 26) and $^{208}\text{Pb}/^{204}\text{Pb}$ from 39.532 (± 72) to 39.600 (± 68) ($n = 11$).

Table 2: Groundmass isotope and whole-rock trace element data of Teide-Pico Viejo succession

Sample	$^{206}\text{Pb}/^{204}\text{Pb}$	$^{207}\text{Pb}/^{204}\text{Pb}$	$^{208}\text{Pb}/^{204}\text{Pb}$	$^{87}\text{Sr}/^{86}\text{Sr}$	$^{143}\text{Nd}/^{144}\text{Nd}$	Pb*	Sr*	Nd*
ABQ-47	19-5050 (22)	15-5919 (22)	39-4490 (68)	0-703118 (22)	2-77	953	60-4	
ARA-01	19-7002 (25)	15-6181 (25)	39-5117 (73)	0-703101 (19)	0-512921 (7)	2-97	875	48-0
ARE-13	19-8133 (23)	15-6248 (23)	39-6045 (69)	0-703116 (26)	0-512940 (9)	2-70	796	51-7
ARE-13 rerun				0-703121 (17)		2-70	796	51-7
BAN-53	19-6773 (23)	15-5929 (21)	39-4962 (64)	0-703138 (26)	0-512905 (22)	2-69	871	45-3
BAN-53 rerun				0-703095 (17)		2-69	871	45-3
BIL-36	19-8142 (23)	15-6350 (21)	39-6282 (65)	0-703072 (19)	0-512991 (25)	2-91	911	48-8
BOT-28	19-7723 (32)	15-6286 (30)	39-6036 (82)	0-703088 (19)	0-512907 (8)	5-84	1116	74-7
CA1-21	19-6737 (24)	15-6040 (23)	39-4959 (64)	0-703099 (22)	0-512916 (9)	3-05	861	48-0
CA2-20	19-7340 (23)	15-6163 (21)	39-5365 (52)	0-703063 (17)	0-512934 (7)	6-50	1124	69-7
CA3-22	19-6932 (25)	15-6114 (23)	39-5215 (63)	0-703115 (17)	0-512913 (14)	3-08	879	48-4
CAN-05	19-7172 (26)	15-6155 (24)	39-5304 (68)	0-703109 (19)	0-512914 (8)	6-06	1101	68-6
CHA-03	19-7388 (26)	15-6139 (25)	39-5570 (69)	0-703119 (19)	0-512931 (7)	7-20	1026	66-8
CHI-01	19-7316 (23)	15-6440 (23)	39-5984 (70)	0-703083 (16)	0-512930 (7)	3-12	1079	56-5
CIO-77	19-7604 (25)	15-6045 (24)	39-5497 (72)	0-703088 (24)	0-512926 (11)	8-29	1011	68-8
CIO-77 rerun	19-7599 (26)	15-6157 (22)	39-5613 (69)			8-29	1011	68-8
COL-15	19-6643 (26)	15-6115 (25)	39-5123 (69)			3-64	863	46-8
CRU-39	19-7625 (23)	15-6128 (23)	39-5644 (69)	0-703071 (19)	0-512964 (7)	5-21	1205	67-5
EST-41	19-7362 (24)	15-6213 (23)	39-5638 (68)	0-703109 (20)	0-512901 (28)	4-09	718	44-7
FAS-02	19-7057 (32)	15-6154 (4)	39-5200 (93)	0-703080 (24)		2-86	907	49-0
GAR-04	19-7663 (23)	15-6231 (22)	39-5824 (65)	0-703116 (20)		2-52	743	43-0
GUA-17	19-6664 (33)	15-6114 (31)	39-5041 (90)	0-703115 (23)		4-24	1046	60-7
HOR-17	19-7365 (26)	15-6191 (27)	39-5454 (72)	0-703082 (20)		5-03	1117	70-7
JEV-03	19-7476 (24)	15-6217 (25)	39-5597 (72)	0-703088 (24)		5-23	1186	72-8
MAR-31	19-7718 (29)	15-6197 (26)	39-5835 (75)	0-703108 (20)	0-512948 (7)	9-44	940	67-1
MNE-33	19-7658 (29)	15-6210 (27)	39-5888 (73)	0-703155 (26)		3-63	949	53-9
MOS-11	19-7340 (18)	15-6245 (17)	39-5222 (51)	0-703173 (26)		3-15	748	45-7
NEG-51	19-6379 (21)	15-6047 (20)	39-5218 (61)	0-703154 (24)		3-02	791	42-1
PAL-56	19-6265 (21)	15-6057 (22)	39-5147 (62)	0-703119 (19)		3-42	1258	73-0
PT-ANT-16	19-7616 (20)	15-6191 (19)	39-5884 (59)	0-703182 (20)		4-98	1268	77-3
PT-EAR-15	19-6987 (19)	15-6082 (18)	39-5218 (54)		0-512919 (9)	4-53	1150	67-8
PV-EAR-13	19-7627 (34)	15-6100 (30)	39-5533 (80)	0-703229 (19)	0-512902 (21)	5-80	1057	60-4
PV-EVO-06	19-8014 (27)	15-6299 (23)	39-6296 (65)	0-703096 (23)	0-512924 (8)	5-44	1031	63-2
PV-INT-09	19-7713 (24)	15-6180 (21)	39-5685 (65)	0-703115 (19)	0-512930 (7)	8-26	1041	69-4
PV-INT-09 rerun	19-7692 (24)	15-6144 (25)	39-5611 (73)			8-26	1041	69-4
RAT-44	19-7696 (24)	15-6149 (25)	39-5648 (71)	0-703105 (23)		6-42	1100	73-2
REV-87	19-7173 (26)	15-6218 (26)	39-5534 (73)	0-703105 (19)	0-512921 (7)	6-11	1112	68-5
SAM-27	19-7740 (26)	15-6457 (24)	39-6289 (68)	0-703040 (22)		4-74	1146	71-22
SIL-60	19-8001 (22)	15-6187 (23)	39-6371 (68)	0-703146 (20)		4-2	1074	69-39
TAC-59	19-7306 (24)	15-6164 (24)	39-6035 (70)			6-03	1343	83-52
TOM-14	19-7179 (21)	15-6085 (20)	39-5177 (57)			7-74	1118	66-83
TOP-55	19-6828 (24)	15-6049 (23)	39-5265 (67)			2-56	927	46-51
TRI-61	19-7570 (24)	15-6179 (24)	39-5624 (75)	0-703128 (20)		4-47	907	68-31
VON-13	19-7888 (35)	15-6152 (29)	39-5828 (80)			6-21	1106	72-91
CIE-18	19-7504 (24)	15-6208 (24)	39-5734 (65)	0-703115 (24)		10-1	419	51-5
CIE-18 rerun				0-703136 (17)		10-1	419	51-5

(continued)

Table 2: Continued

Sample	$^{206}\text{Pb}/^{204}\text{Pb}$	$^{207}\text{Pb}/^{204}\text{Pb}$	$^{208}\text{Pb}/^{204}\text{Pb}$	$^{87}\text{Sr}/^{86}\text{Sr}$	$^{143}\text{Nd}/^{144}\text{Nd}$	Pb*	Sr*	Nd*
COR-05	19-7494 (27)	15-6233 (26)	39-5780 (78)	0-703127 (22)	0-512951 (11)	13-2	864	57-88
CUE-14	19-7793 (27)	15-6221 (25)	39-5752 (77)	0-703120 (19)	0-512916 (8)	15-96	767	58-48
CUE-14 rerun	19-7669 (28)	15-6102 (24)	39-5537 (71)			15-96	767	58-48
LEN-15	19-7744 (24)	15-6226 (24)	39-5917 (69)	0-703107 (17)	0-512956 (14)	13-09	323	49-22
PO1-06	19-7705 (31)	15-6208 (28)	39-5933 (82)	0-703094 (20)		13-2	862	57-3
PO2-09	19-7586 (20)	15-6184 (21)	39-5762 (61)	0-703095 (19)		n.a.	n.a.	n.a.
PT-INE-11	19-7609 (25)	15-6120 (22)	39-5633 (62)	0-703178 (17)	0-512923 (6)	14-7	261	38-4
PV-LAT-01	19-7612 (25)	15-6160 (21)	39-5654 (61)	0-703399 (23)	0-512924 (45)	14-98	360	58-21
REV-85	19-7688 (25)	15-6186 (24)	39-5776 (67)			14-73	184	47-66
VER-32	19-7667 (29)	15-6337 (28)	39-6068 (80)	0-703135 (17)		11-8	302	51-7
ABA-36	19-7618 (26)	15-6095 (24)	39-5630 (64)			19-3	5-5	56
ABB-19	19-7648 (22)	15-6143 (23)	39-5713 (65)			19-2	7-2	57-5
BOQ-13	19-7623 (26)	15-6047 (25)	39-5316 (73)	0-704083 (20)		19-8	3-3	55-3
BOQ-13 rerun				0-704083 (20)		19-8	3-3	55-3
CAB-27	19-7635 (26)	15-6084 (24)	39-5549 (69)	0-703395 (23)	0-512938 (8)	17-6	34-2	44-1
MAJ-17	19-7680 (29)	15-6175 (27)	39-5838 (75)	0-703321 (19)		17-64	34-94	53-89
MB5-05	19-7660 (25)	15-6141 (20)	39-5713 (67)			18-97	9-63	57-22
MB7-08	19-7817 (25)	15-5289 (23)	39-6002 (69)	0-704900 (16)		20-95	8-22	56-84
MB8-06	19-7578 (26)	15-6056 (25)	39-5474 (73)		0-512945 (23)	21-45	2-41	61-93
PT-LAE-04	19-7541 (29)	15-6064 (25)	39-5379 (65)	0-703091 (2)	0-512940 (6)	16-1	117	50
RBL-01	19-7585 (28)	15-6171 (24)	39-5645 (69)	0-703275 (17)	0-512926 (8)	19-2	3-8	57-4
PT-SUM-01	19-7657 (30)	15-6130 (28)	39-5758 (79)		0-512950 (17)			
FU-Msed-PtoP II-1	19-7448 (3)	15-6269 (28)	39-6810 (84)	0-703473 (21)				
FU-Msed-PtoP II-5	19-4369 (28)	15-6516 (25)	39-4798 (76)					
FU-Msed-I-1	18-8000 (27)	15-6713 (27)	39-0664 (79)					
FV-Msed-D1-PtoP	19-0767 (31)	15-6767 (30)	39-4150 (86)	0-707684 (21)				
FU-PLK-PtoP-II	18-5307 (63)	15-6263 (54)	38-2679 (141)					

n.a., not available. Results from groundmass isotope analyses. All errors are 2 SD. Classification of samples according to trace element geochemistry in right hand column. *Whole-rock trace element data from Rodriguez-Badiola *et al.* (2006).

The transitional and felsic lavas show a distinctive behaviour in their $^{206}\text{Pb}/^{204}\text{Pb}$ ratio compared with the mafic lavas. In a plot of $^{206}\text{Pb}/^{204}\text{Pb}$ vs $^{207}\text{Pb}/^{204}\text{Pb}$ (Fig. 5), the mafic lavas trend along the Northern Hemisphere Reference Line (NHRL; $\Delta^{206}\text{Pb}/^{204}\text{Pb}_{\text{max-min}} = 0.3048$), consistent with literature data for Tenerife (Fig. 5). In turn, the transitional and felsic lavas are confined to a narrow $\Delta^{206}\text{Pb}/^{204}\text{Pb}_{\text{max-min}}$ of 0.0250 and 0.0275, respectively, which translates to 8.2% and 9% of the total mafic range observed (Table 3).

Additional features of the dataset are the very low $^{207}\text{Pb}/^{204}\text{Pb}$ detected in sample MB7, which, however, is well within the range of published Tenerife data, and, for historical lavas, higher $^{207}\text{Pb}/^{204}\text{Pb}$ values than those reported by Simonsen *et al.* (2000) [15.614 (± 25)–15.644 (± 23) vs 15.586–15.590 (no errors reported)]. Overall, the Sr–Nd–Pb isotopic results match existing literature data

for Tenerife (Palacz & Wolff, 1989; Simonsen *et al.*, 2000; Abratis *et al.*, 2002; Gurenko *et al.*, 2006).

Oxygen isotope composition of feldspar and groundmass

Fifteen $\delta^{18}\text{O}$ measurements were performed on feldspar. Teide–Pico Viejo feldspars exhibit oxygen isotope ratios between 5.43 and 5.99‰ that positively correlate with SiO_2 , except for one outlier. Feldspars from the mafic lavas range from $5.43 \pm 0.11\%$ to $5.84 \pm 0.02\%$. Feldspars from the transitional lavas range from $5.82 \pm 0.29\%$ to $5.88 \pm 0.11\%$, except for the above-mentioned outlier at $5.46 \pm 0.11\%$ (LAJ-24, Montaña Las Lajas). The felsic lavas have feldspar oxygen ratios that range from $5.88 \pm 0.11\%$ to $5.99 \pm 0.11\%$ (i.e. defining a very narrow compositional range). The $\delta^{18}\text{O}$ in Teide–Pico Viejo feldspars thus range upwards from just below the mid-ocean

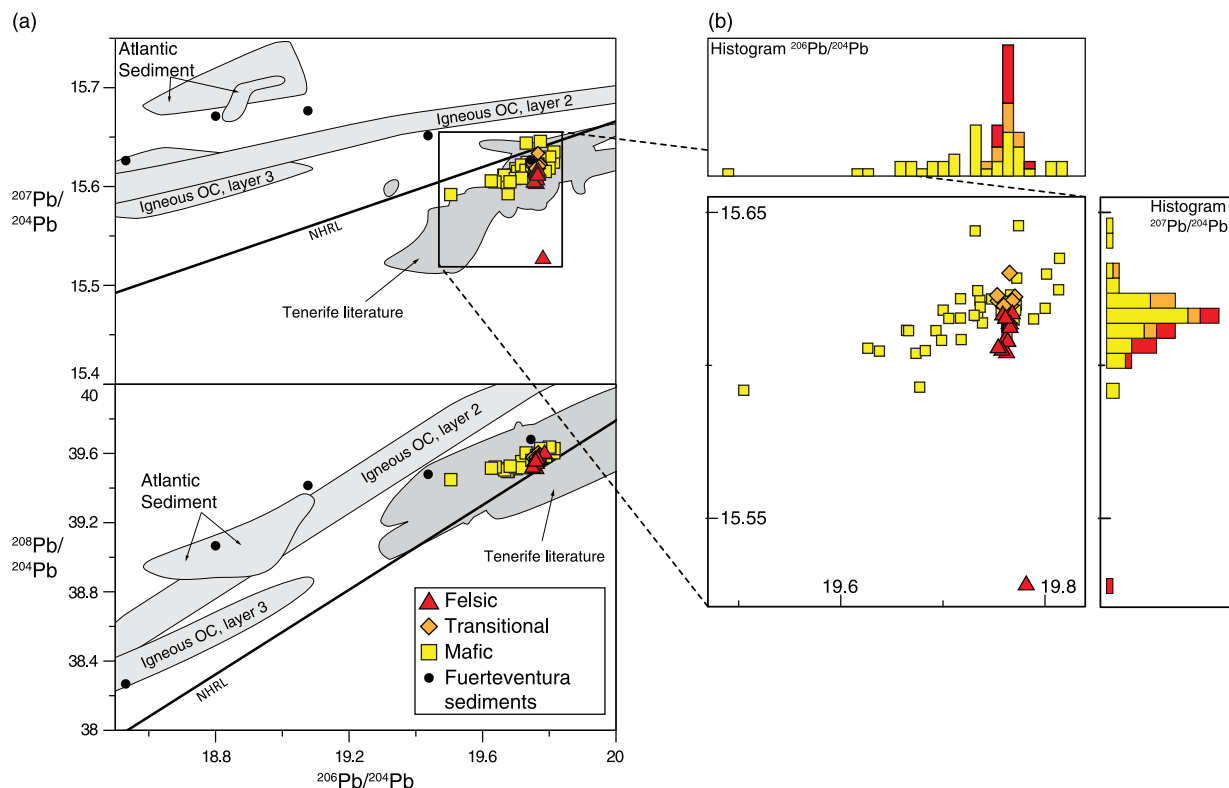


Fig. 5. (a) Pb isotope compositions of Teide–Pico Viejo magmatic rocks compared with literature data (fields). All errors are 2SD and included in the symbols. Northern Hemisphere Reference Line (NHRL) after Hart (1984). The dark grey field represents combined data for the Tenerife shield volcanoes Anaga and Teno, Tenerife slope dredges and Las Cañadas lavas (Sun, 1980; Simonsen *et al.*, 2000; Abratis *et al.*, 2002; Gurenko *et al.*, 2006). The light grey fields represent data for the oceanic crust (OC) and Atlantic sediments (Sun, 1980; Hoernle *et al.*, 1991; Hoernle, 1993). It should be noted that Atlantic sediment compositions do not appear to have influenced the Teide–Pico Viejo succession. (b) Close-up of the Teide–Pico Viejo data combined with histograms of $^{206}\text{Pb}/^{204}\text{Pb}$ and $^{207}\text{Pb}/^{204}\text{Pb}$ ratios in the Tenerife post-collapse lavas.

Table 3: $\Delta\text{Pb}–\text{Pb}_{\text{max–min}}$ ranges in compositional groups

	$\Delta^{206}\text{Pb}/^{204}\text{Pb}_{\text{max–min}}$	$\Delta^{207}\text{Pb}/^{204}\text{Pb}_{\text{max–min}}$	$\Delta^{208}\text{Pb}/^{204}\text{Pb}_{\text{max–min}}$
Primitive	0.3092 (12)	0.0538 (12)	0.1881 (34)
Transitional	0.0250 (13)	0.0235 (14)	0.0531 (40)
Evolved	0.0275 (14)	0.0886 (13)	0.0685 (36)

$\Delta^{20x}\text{Pb}/^{204}\text{Pb}_{\text{max–min}}$ values for all three compositional groups were calculated following: $(\Delta^{20x}\text{Pb}/^{204}\text{Pb}_{\text{max}}) - (\Delta^{20x}\text{Pb}/^{204}\text{Pb}_{\text{min}})$. The larger error of the maximum and minimum Pb isotope values is given in parentheses. Compared with the mafic lavas, the transitional and felsic lavas show limited variation in $^{206}\text{Pb}/^{204}\text{Pb}$ (low $\Delta^{206}\text{Pb}/^{204}\text{Pb}$ value).

ridge basalt (MORB) array (Taylor & Sheppard, 1986) and form a broadly linear trend up to $\sim 6\%$ that correlates with decreasing MgO concentrations.

We also carried out six $\delta^{18}\text{O}$ analyses of groundmass separates. Groundmass values are higher, ranging from 5.59

to $6.80 \pm 0.11\%$, and loosely increase with decreasing MgO. Two groundmass analyses of mafic lavas resulted in values of $5.59 \pm 0.11\%$ and $5.73 \pm 0.11\%$. Two transitional groundmass samples yielded $\delta^{18}\text{O}$ values of $6.00 \pm 0.11\%$ and $6.80 \pm 0.11\%$. Two groundmass analyses of felsic lavas produced values of $5.81 \pm 0.11\%$ and $6.23 \pm 0.11\%$ (Table 4).

The six groundmass analyses correspond to six of the 15 feldspar analyses. In samples LEN (transitional) and MAJ (felsic) the feldspar crystals have a lower $\delta^{18}\text{O}$ ratio than their host groundmass. In sample MAR (mafic) feldspar is higher in $\delta^{18}\text{O}$, and in samples RAT (mafic), PT-INE (transitional) and RBL (felsic) the values overlap within error. When calculating the theoretical equilibrium values of groundmass (melt) $\delta^{18}\text{O}$ from the feldspar ratio after Bindeman *et al.* (2004), five out of six pairs are in disequilibrium (Table 4). Only sample PT-INE indicates an equilibrium between feldspar and groundmass. The disequilibrium observed between the majority of feldspar–groundmass pairs indicates that either (1) the groundmass has undergone greater postmagmatic secondary alteration after eruption, (2) the feldspars analysed are xenocrysts

Table 4: Feldspar and groundmass oxygen isotope data of Teide–Pico Viejo succession

	$\delta^{18}\text{O}$ feldspar (‰, SMOW)	Error feldspar (\pm ‰)	$\delta^{18}\text{O}$ groundmass (‰, SMOW)	Error groundmass (\pm ‰)	$\Delta\delta^{18}\text{O}_{\text{fsp-gm}}$ (‰)	Comments
<i>Primitive</i>						
CA1-23	5.43	0.11				
CIO-77	5.84	0.02				average
MAR-37	5.83	0.11	5.59	0.11	0.24	
PV-EAR-15	5.815	0.17				average
PV-INT-08	5.78	0.11				average
RAT-84	5.75	0.11	5.73	0.11	0.02	
<i>Transitional</i>						
CUE-14	5.875	0.03				average
LAJ-23	5.46	0.11				
LEN-15	5.88	0.11	6.80	0.11	0.92	
PT-INE-17	5.86	0.11	6.00	0.11	0.14	
PV-LAT-04	5.82	0.09				average
PV-LAT-66	5.82	0.09				average
<i>Evolved</i>						
MAJ-17	5.88	0.11	6.23	0.11	0.35	
PT-LAE-02	5.99	0.11				
RBL-02	5.98	0.11	5.81	0.11	0.17	

Oxygen isotope values of feldspar and corresponding groundmass separates grouped according to trace element chemistry. Several feldspars have been analysed twice, and an average is given in these cases.

and bear no direct genetic relationship to the host rocks in which they are found, or (3) a change in the $\delta^{18}\text{O}$ ratio has occurred within these magmas after feldspars crystallized (e.g. Bindeman, 2008). We cannot estimate the extent of these possibilities other than saying that the groundmass samples appear fresh. None the less, we choose to discuss the $\delta^{18}\text{O}$ of the feldspars as a better proxy for the $\delta^{18}\text{O}$ value of the ambient melt.

DISCUSSION

The radiogenic and stable isotope compositions of the Teide–Pico Viejo lavas permit qualitative deductions about the open-system behaviour of the magmatic plumbing system. Isotope mixing models demonstrate systematic isotopic variations within the Teide–Pico Viejo succession and thus can be used to constrain the composition of the potential assimilated. The protolith and the degree of partial melting necessary to explain the observed variations is determined using the REE data of Rodríguez-Badiola *et al.* (2006). Our preferred model involves an assimilation and fractional crystallization scenario. To quantify magmatic differentiation processes an energy-constrained (EC), combined assimilation-fractional crystallization (AFC) model was calculated. Based on these results the potential for crustal melting and implications for

magmatic differentiation in oceanic island plumbing systems are discussed.

An open system at Teide–Pico Viejo

The bulk of our lava samples have uniform $^{87}\text{Sr}/^{86}\text{Sr}$ ratios of 0.7031–0.7033. Two lavas, both phonolites from the felsic group, exceed this Sr isotope baseline with ratios extending up to 0.7049. This probably demonstrates the potential for open-system behaviour within the Teide–Pico Viejo succession. Although elevated Sr isotope ratios may also develop by radiogenic ingrowth, at Teide–Pico Viejo this is precluded by the limited time-scales available for closed-system fractionation. Hawkesworth *et al.* (2000) used U–Th series isotopic data to suggest that, in Tenerife, a hypothetical closed-system magma chamber would take 230 ± 70 kyr for basanite magma to fractionate to residual phonolite. This is too short to create $^{87}\text{Sr}/^{86}\text{Sr}$ ratios of up to 0.7049 by radioactive decay alone and the involvement of a high $^{87}\text{Sr}/^{86}\text{Sr}$ component must be considered. This implies an open-system for the Teide–Pico Viejo magmatic system.

Because the mantle source of the primary Tenerife basalts is thought to be of uniformly low $^{87}\text{Sr}/^{86}\text{Sr}$ composition (Simonsen *et al.*, 2000), how may elevated Sr isotope ratios have formed in Tenerife?

First, relatively old, highly evolved bodies of rock with low Sr concentrations and high Rb/Sr ratios have a high rate of ingrowth of ^{87}Sr . For example, a syenite with an Rb/Sr ratio of 16 (e.g. Wolff & Storey, 1984; Wolff & Palacz, 1989) would need less than 3 Myr to have its Sr isotope composition evolve from 0.703 to 0.705 (see Halliday *et al.*, 1989; Christensen & DePaolo, 1993). Rocks of comparable composition are present throughout the 12 Myr record of subaerial Tenerife magmatism, including the Roque Del Conde shield stage.

Second, the Jurassic oceanic crust below Tenerife is overlain by a thick sedimentary sequence with elevated $^{87}\text{Sr}/^{86}\text{Sr}$ through which the primitive magma would have to pass (Hoernle *et al.*, 1991). Plausibly, this high $^{87}\text{Sr}/^{86}\text{Sr}$ sediment may have contaminated the Tenerife magmas during their ascent. Additionally, hydrothermal circulation could leach these ocean floor sediments and transport high $^{87}\text{Sr}/^{86}\text{Sr}$ fluids upwards through the stratigraphy.

Third, syn-eruptive seawater contamination of submarine lavas may occur. For example, in lavas from the Axial Seamount, Juan de Fuca Ridge, the compositional signature of seawater can be traced within pillow rims to ~1 cm depth (Schiffman *et al.*, 2010). Thus, seawater contamination may introduce significant compositional heterogeneities during the submarine growth of an oceanic island. The rocks contaminated by seawater during the seamount stage are either still present or could have been reworked by subsequent magmatic activity (see Hansteen & Troll, 2003).

We suggest that early sediment incorporation, seamount–seawater interaction and/or radiogenic ingrowth must all be considered possible. Notably, in all these processes the generation of highly radiogenic Sr isotope ratios occurs at crustal levels and is unrelated to mantle metasomatism. In Tenerife, isotopic heterogeneities in $^{87}\text{Sr}/^{86}\text{Sr}$ are thus probably of crustal origin. In the discussion that follows, the variations detected in the radiogenic isotope compositions of Nd and Pb are used to further constrain the composition of the crustal component.

Sediment contamination

Felsic Teide–Pico Viejo lavas are markedly different in their Pb isotope composition compared with the mafic lavas. Consistent with literature data, the mafic lavas delineate a field of ‘baseline’ Pb isotope ratios, parallel to the NHRL on Pb–Pb isotope diagrams (Fig. 5). This has to be considered to reflect the natural variability in the mantle source (see Simonsen *et al.*, 2000). The felsic lavas, in contrast, define a very narrow, vertical trend, characterized by a uniform $^{206}\text{Pb}/^{204}\text{Pb}$ ratio but very variable $^{207}\text{Pb}/^{204}\text{Pb}$ ratios, which are more variable than those of the mafic lavas. Both $^{206}\text{Pb}/^{204}\text{Pb}$ and $^{207}\text{Pb}/^{204}\text{Pb}$ variations in the felsic lavas are consistent with the total range of Pb isotope data so far reported for Tenerife rocks, including the sample MB7 (Montaña Blanca) with the lowest

$^{207}\text{Pb}/^{204}\text{Pb}$ value (Fig. 5). As there are no indications for any error during sample preparation or measurement, the Pb isotope ratios of this sample have to be considered real.

The combination of a uniform, high $^{206}\text{Pb}/^{204}\text{Pb}$ and a very low $^{207}\text{Pb}/^{204}\text{Pb}$ in the felsic lavas is a new observation and distinct from the compositions of the mafic lavas. The Pb–Pb isotope variations therefore demonstrate that the Teide–Pico Viejo succession has formed by open-system processes. An assimilated or component with uniform, high $^{206}\text{Pb}/^{204}\text{Pb}$ but low $^{207}\text{Pb}/^{204}\text{Pb}$ must have been involved in the formation of the felsic lavas (Fig. 5). An assimilated that is potentially present during magma ascent in the Canaries is Atlantic sediment or uplifted and altered sediment in the island’s basement. Atlantic sediments generally plot at lower $^{206}\text{Pb}/^{204}\text{Pb}$ and much higher $^{207}\text{Pb}/^{204}\text{Pb}$ compositions (Sun, 1980; Hoernle *et al.*, 1991; Hansteen & Troll, 2003). Because of their Pb concentrations, contamination by sediments would have a strong effect on the Pb isotope trends defined by the Teide–Pico Viejo lavas. However, no such trend toward sediments is discernible in the Teide–Pico Viejo succession. Atlantic sediments are thus unlikely to have influenced the Pb isotope compositions of the Teide–Pico Viejo lavas directly (Fig. 5). In contrast, the mafic members of the pre-Teide, Quaternary Diego Hernández Formation and the Las Cañadas Volcano sequence do meet the assimilated requirements of low $^{207}\text{Pb}/^{204}\text{Pb}$ and high $^{206}\text{Pb}/^{204}\text{Pb}$ (Simonsen *et al.*, 2000), highlighting the potential for a suitable assimilated being present below Teide. The combination of Sr and Pb isotope data indicates that Atlantic sediments are unlikely to be a major, direct assimilated in the petrogenesis of the Teide–Pico Viejo succession.

Neodymium isotope ratios

Similar to the $^{206}\text{Pb}/^{204}\text{Pb}$ ratios, the Teide–Pico Viejo Nd isotope ratios become more uniform with increasing degree of differentiation (Fig. 6). This can be interpreted in two ways: either a dominant signal in the mantle source, which is preserved by chance in the felsic magmas, or reworking of crustal material where the $^{143}\text{Nd}/^{144}\text{Nd}$ of the assimilated dominates in the more differentiated lavas. In the light of the Sr and Pb isotopic data, which indicate an open-system at Teide–Pico Viejo, the latter appears more likely. In consequence, the assimilated is probably of uniform Nd isotope composition, in a range comparable with the $^{143}\text{Nd}/^{144}\text{Nd}$ ratios measured in the felsic lavas (0.512924–0.512950).

Large-scale crustal assimilation in the formation of felsic lavas?

Sr–Nd isotope mixing models allow us to test whether or not involvement of an assimilated with high $^{87}\text{Sr}/^{86}\text{Sr}$ and uniform $^{143}\text{Nd}/^{144}\text{Nd}$ can reproduce the Sr and Nd isotope variations observed at Teide–Pico Viejo. Because the mafic lavas have variable Nd isotope ratios, several of these

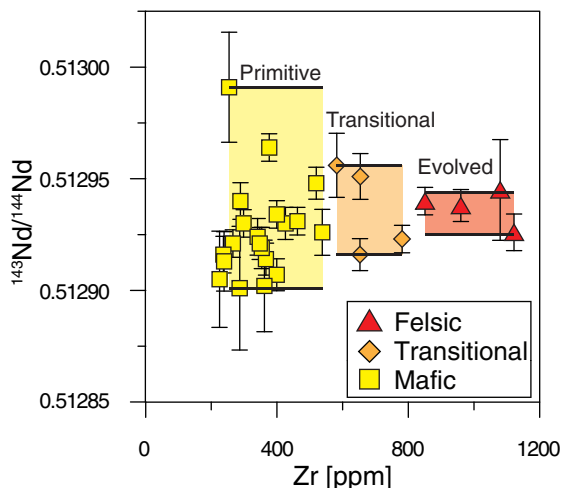


Fig. 6. Variation of $^{143}\text{Nd}/^{144}\text{Nd}$ for Teide–Pico Viejo lavas vs Zr concentration as a differentiation index. Errors are 2SD.

lavas have been combined with a high $^{87}\text{Sr}/^{86}\text{Sr}$ assimilant of uniform Nd isotope composition.

When employing pre-existing data from Tenerife to characterize the assimilant, the only deposit with high enough $^{87}\text{Sr}/^{86}\text{Sr}$ (>0.7049) is the ~ 570 ka Granadilla ignimbrite, a caldera-forming event within the Upper Group of the Las Cañadas edifice (Martí *et al.*, 1994, 1997; Bryan *et al.*, 1998). No other analysed samples have the isotopic compositions expected of the high $^{87}\text{Sr}/^{86}\text{Sr}$ assimilant. Granadilla pumice clasts have yielded whole-rock Sr and Nd isotope ratios of 0.70356–0.70571 and 0.512825–0.512892, respectively (Palacz & Wolff, 1989). However, using the Granadilla data as the assimilant composition (combined with low Sr/Nd Teide–Pico Viejo felsic lavas) does not reproduce the compositional trend of the felsic lavas because the $^{143}\text{Nd}/^{144}\text{Nd}$ ratios of the Granadilla pumice are too low (Fig. 7). Combining this assimilant with high Sr/Nd lavas as the mafic end-member produces even less suitable mixing hyperbolae. This is consistent with the Pb isotope composition of the Granadilla ignimbrite, which is lower in $^{206}\text{Pb}/^{204}\text{Pb}$ than the felsic lavas (19.621–19.734 vs 19.754–19.782; Palacz & Wolff, 1989). Thus, assimilation of a component with the isotopic composition of the Granadilla ignimbrite is unlikely to have been involved in the formation of the high $^{87}\text{Sr}/^{86}\text{Sr}$ felsic Teide–Pico Viejo magmas.

The assimilant composition is, however, constrained by the isotopic data in that it must have had a higher $^{87}\text{Sr}/^{86}\text{Sr}$ ratio than sample MB7 (0.7049). Furthermore, the assimilant needs to have a $^{206}\text{Pb}/^{204}\text{Pb}$ value similar to the uniform $^{206}\text{Pb}/^{204}\text{Pb}$ ratios observed in the felsic lavas, but its $^{207}\text{Pb}/^{204}\text{Pb}$ must be lower. Its Nd isotope composition must be similarly uniform to what is observed in the felsic Teide lavas. Such compositional characteristics are observed within several deposits of the Las Cañadas

Volcano, the 3 Myr sequence that underlies Teide–Pico Viejo. The Granadilla ignimbrite displays appropriate Sr isotope ratios (Palacz & Wolff, 1989). The Diego Hernández Formation basalts have suitable Pb isotope ratios, except for sample MB7, which has a lower $^{207}\text{Pb}/^{204}\text{Pb}$ value, and mafic Las Cañadas rocks have appropriate $^{143}\text{Nd}/^{144}\text{Nd}$ values (Simonsen *et al.*, 2000).

Using a hypothetical assimilant of the required composition in mixing models provides further constraints for the differentiation processes at work. The hypothetical assimilant was constructed as follows: because in Tenerife, high $^{87}\text{Sr}/^{86}\text{Sr}$ ratios have been found only in highly differentiated rocks (number of $^{87}\text{Sr}/^{86}\text{Sr}$ analyses $n = 153$; Palacz & Wolff, 1989; Simonsen *et al.*, 2000; Abratis *et al.*, 2002; Gurenko *et al.*, 2006), data for the felsic Granadilla ignimbrite of Palacz & Wolff (1989) were used as a starting point. These data were then modified with higher $^{143}\text{Nd}/^{144}\text{Nd}$ and suitable $^{206}\text{Pb}/^{204}\text{Pb}$ values to meet the compositional requirements for the hypothetical assimilant. The arithmetic mean $^{143}\text{Nd}/^{144}\text{Nd}$ value (0.512937, $n = 6$) and the $^{206}\text{Pb}/^{204}\text{Pb}$ ratios of the felsic lavas were used to obtain an estimate of the Nd and Pb isotope composition. We used comparable Sr and Nd concentrations and, consequently, a low Sr/Nd ratio in the hypothetical assimilant, which therefore bears the Sr, Nd and Pb signatures of Tenerife highly differentiated rocks. Several mafic end-members were used in these models to account for the variability in Nd isotope ratios observed in mafic Teide lavas. The resulting mixing hyperbolae, which on the Nd–Sr isotope diagram also provide an approximation to assimilation paths, not only encompass the felsic lavas within a single mixing relationship, but also include all transitional and mafic lavas; that is, the entire differentiation sequence from mafic to felsic compositions (Fig. 7).

The significance of this is two-fold: first of all, it demonstrates a strong genetic relationship for all Teide–Pico Viejo lavas, which implies that for comparable compositions comparable pressure–temperature paths were followed and very similar material may have been assimilated throughout the history of Teide–Pico Viejo magma evolution. Second, the curvatures of the mixing hyperbolae require a low Sr/Nd ratio in the assimilant, which provides strong evidence for the involvement of an assimilant of felsic composition, because an assimilant of higher Sr/Nd ratio would cause the mixing hyperbolae to plot through empty space. To have significant impact on the magma composition, the assimilant must have limited compositional variability and a felsic composition.

These findings hold true for Sr concentrations in the mafic starting composition of as low as 117 ppm. An assimilant with a high Sr concentration would of course affect the $^{87}\text{Sr}/^{86}\text{Sr}$ of the magma more efficiently; however, igneous rocks with both high Sr concentrations and elevated $^{87}\text{Sr}/^{86}\text{Sr}$ are not observed in Tenerife ($n = 153$;

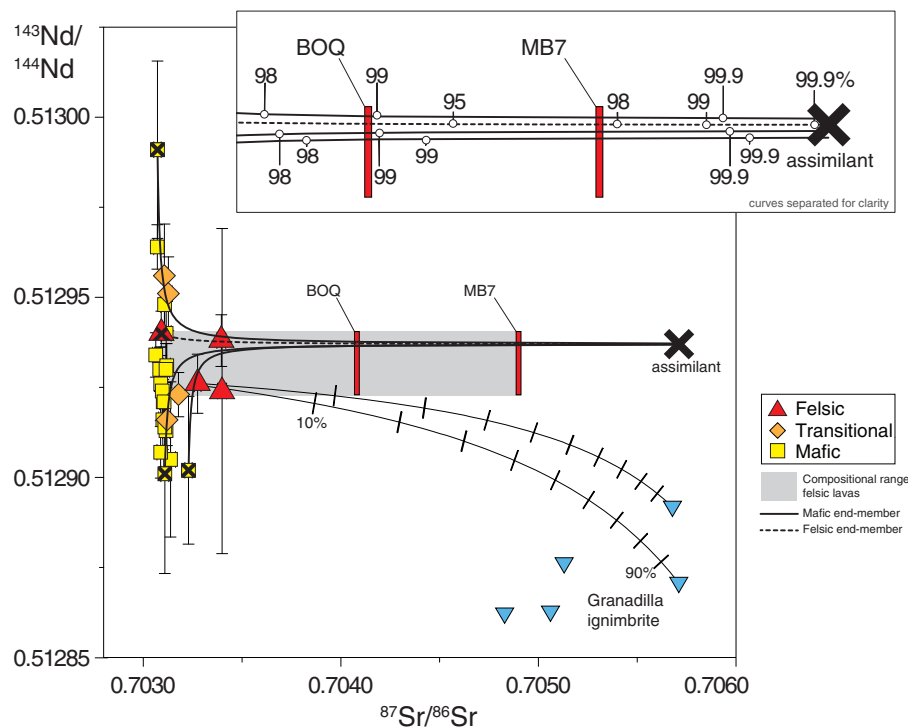


Fig. 7. Variation of $^{87}\text{Sr}/^{86}\text{Sr}$ vs $^{143}\text{Nd}/^{144}\text{Nd}$ for Teide–Pico Viejo lavas compared with data for the Granadilla ignimbrite (Palacz & Wolff, 1989). The assimilant is approximated (black cross) using the composition of the Granadilla ignimbrite sample with the highest $^{87}\text{Sr}/^{86}\text{Sr}$ ratio, combined with the arithmetic mean of the $^{143}\text{Nd}/^{144}\text{Nd}$ ratios of the felsic lavas. Four representative mixing hyperbolae are illustrated between the hypothetical assimilant and three mafic lavas and one felsic lava (black curves). Inset shows curves vertically separated for better readability. It should be noted that all curves trend towards the same assimilant composition. Numbers indicate percentage of assimilant involved in the mixture. Hyperbolae for all remaining RBL calculations are shown in the inset, except for sample PV-LAT-01, for which there are no compositional data available. The curve for RBL-02 and the assimilant deviates from the general pattern observed. Instead of representing a suitable uncontaminated magma, sample RBL-02 itself shows evidence of magma mixing. It should be noted that to model successfully sample MB7, between 97.8 and 99.5% of assimilant is required.

Palacz & Wolff, 1989; Simonsen *et al.*, 2000; Abratis *et al.*, 2002; Gurenko *et al.*, 2006; this study). The strong influence of a felsic component was further tested by using an artificially high $^{87}\text{Sr}/^{86}\text{Sr}$ ratio of 0.708 in the assimilant (never observed in Tenerife), but even then 92.1% assimilant or felsic component is required to obtain the isotopic composition of sample MB7.

The isotopic compositions of the Teide–Pico Viejo felsic lavas therefore display a strong influence of a highly differentiated, high $^{87}\text{Sr}/^{86}\text{Sr}$ assimilant that appears to become more dominant with increasing degree of differentiation. The important question of whether this assimilant is a partial melt of felsic composition that originated from a crustal protolith or a bulk melt of a felsic protolith will be addressed after further narrowing down the characteristics of the protolith by interpretation of the available oxygen isotope data.

Oxygen isotope heterogeneity of the assimilant

At Teide–Pico Viejo, the variations in feldspar and groundmass $\delta^{18}\text{O}$ appear relatively scattered with excursions to

high and low values (Fig. 8). Closed-system fractional crystallization is thought to continually raise $\delta^{18}\text{O}$ values with differentiation (see grey shaded fields in Fig. 8; Bindeman, 2008), whereas uptake of non-magmatic material usually generates a deviation from this trend. For example, at Krafla volcano (Iceland), assimilation of hydrothermally altered country-rocks led to a decrease of $\delta^{18}\text{O}$ with increasing differentiation (Nicholson *et al.*, 1991). At Teide–Pico Viejo, most of the data plot at the lower end of the range within error of the closed-system field for the alkali-rich series, with three samples yielding significantly lower values. Additionally, two of the most evolved rocks have groundmass compositions with much higher $\delta^{18}\text{O}$ values, which are not reproduced by the feldspar crystals hosted in these samples. This may be indicative of either secondary alteration of the groundmass or late-stage addition of a high- $\delta^{18}\text{O}$ component to the melt. As we found no evidence for alteration our preferred interpretation is assimilation of materials of variable oxygen isotope composition. This, in turn, is consistent with open-system behaviour as required by the radiogenic isotopes.

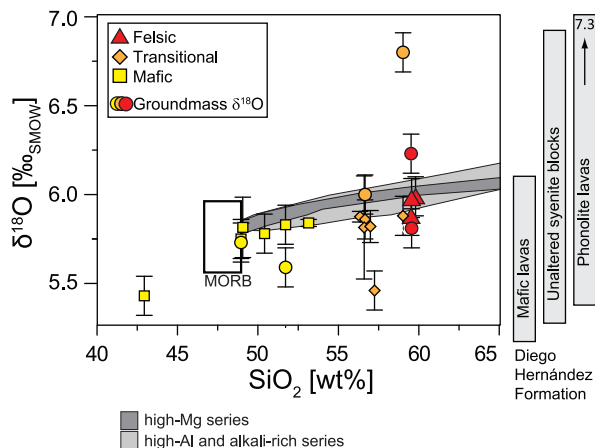


Fig. 8. Oxygen isotope ratios of feldspar and groundmass separates vs whole-rock SiO_2 content. Grey shaded arrays denote closed-system oxygen isotope fractionation (from Bindeman, 2008). Teide–Pico Viejo data deviate from these arrays and thus demonstrate open-system behaviour. To the right: grey bars are data from Wolff *et al.* (2000) for the Diego Hernández Formation. These data overlap with the range of values found in Diego Hernández ignimbrites and nepheline syenites, consistent with Diego Hernández-type rocks being a potential assimilant.

Lithic blocks in pre-Teide deposits constrain the types of rock that exist at depth in the Tenerife volcanic plumbing system. These lithic blocks hosted in ignimbrites are dominantly of nepheline syenite composition and are interpreted to be co-genetic intrusive remnants of these felsic ignimbrites (Wolff *et al.*, 2000; Edgar *et al.*, 2002, 2007). These exhumed nepheline syenite blocks therefore probably reflect the country-rock available for assimilation at depth. In these fresh to variously altered nepheline syenite blocks, Wolff *et al.* (2000) detected heterogeneous $\delta^{18}\text{O}$ values, which entirely overlap with the values observed for the Teide–Pico Viejo succession (Fig. 8). Considering that each feldspar–groundmass pair represents a single eruption, separate in space and time from every other eruption, it is conceivable that different eruptions sampled distinct portions of the nepheline syenite that had previously been altered to different degrees resulting in different $\delta^{18}\text{O}$ compositions. We therefore argue that the unsystematic variations of $\delta^{18}\text{O}$ feldspar values in the Teide–Pico Viejo lavas may have been caused by assimilation of both high- $\delta^{18}\text{O}$ and low- $\delta^{18}\text{O}$ nepheline syenites, previously altered by variable degrees at low and high temperatures respectively. Thus, the resulting heterogeneity in the $\delta^{18}\text{O}$ composition of the assimilant was inherited in variable proportions by the different lavas of the Teide–Pico Viejo succession. As minor amounts of alteration by meteoric water do not alter radiogenic isotopes, the scattered variations in $\delta^{18}\text{O}$ values observed in Teide–Pico Viejo lavas do not affect the systematic behaviour of the radiogenic isotopes.

Geothermobarometry calculations and phase equilibria studies further support a nepheline syenite protolith for

the assimilant in our model. Crystallization depths inferred from phase equilibria, melt inclusion analysis and geothermobarometry indicate shallow storage of the felsic magmas on Tenerife. For example, the experimental results of Wellman (1970) suggest that the phase assemblage of the nepheline syenites forms at less than 160 MPa. Specifically for the pre-Teide ignimbrite, biotite–sanidine–magnetite equilibria indicated crystallization at 130–240 MPa (Wolff & Storey, 1983; Wolff, 1987). Phase equilibrium experiments constrain the phase assemblage of the Teide phonolites to crystallize at 150 MPa (Andújar *et al.*, 2010). Hygrometry and phonolite melt inclusion data from Teide–Pico Viejo yield minimum pressures of 70–150 MPa (Ablay *et al.*, 1998). Thus the Teide phonolites appear to have crystallized at the same crustal depth as the nepheline syenites of the pre-Teide cycles. For comparison, Canary Island primitive lavas show main crystallization levels at Moho depths or somewhat shallower at ~8–10 km (e.g. Klügel *et al.*, 2005; Galipp *et al.*, 2006; Longpré *et al.*, 2008; Stroncik *et al.*, 2009). Larger degrees of assimilation may thus be precluded by the fast ascent of these magmas through the rift zones (i.e. as dykes), although differentiation to intermediate compositions can still be achieved at greater depth by crystal–liquid fractionation.

These lines of evidence therefore support the proposal based on the isotopic constraints that highly differentiated intrusive material represents the key protolith for recycling within the Teide–Pico Viejo volcano. Overall, pre-Teide nepheline syenites best meet the requirements for the protolith of the Teide–Pico Viejo assimilant based on radiogenic and stable isotope systematics, trace element ratios, geobarometric and phase equilibrium data. The extent to which protolith must have been melted during assimilation will be established below.

Wholesale melting of nepheline syenite?

The composition of a partial melt of the country rock is strongly affected by the degree of partial melting. Because incompatible trace elements are strongly partitioned into the melt phase during partial melting, trace element ratios allow discrimination between assimilation of (1) a component of juvenile composition, which previously existed as pod of melt and was incorporated by magma mixing, and (2) the assimilation of a partial melt of the country-rock (defined *sensu stricto* as the wall-rock that is being intruded, including previous magma that had solidified to form igneous rock). For example, the uptake of a 10% partial melt of nepheline syenite will produce very different trace element ratios compared with assimilating a bulk-melt of the same rock composition.

At a given mafic starting composition and a fixed amount of assimilant, AFC-related variations in REE ratios are mainly controlled by the degree of partial melting of the assimilant. This is because the REE are little

fractionated during the crystallization of basanite magmas, such that fractional crystallization cannot be identified using REE ratios (Schnetzer & Philpotts, 1970; Lemarchand *et al.*, 1987; Adam & Green, 2006). Hence, it is adequate to approximate the degree of partial melting of the assimilated by calculating binary mixing models involving incompatible trace element ratios, despite the minor effects of simultaneous fractional crystallization. In binary mixing models expressed in terms of REE ratios, lower degrees of partial melting of the protolith enrich the more incompatible element in an REE ratio and thus cause higher La/Sm and Gd/Yb ratios in the assimilated.

The binary mixing models calculated combine partial melts of nepheline syenite with Teide mafic melt compositions. It was tested if the REE ratios of the Teide–Pico Viejo felsic lavas could be reproduced by varying the degree of partial melting of the protolith (i.e. nepheline syenite). The end-member compositions used are Teide–Pico Viejo whole-rocks (Rodríguez-Badiola *et al.*, 2006) and Diego Hernández nepheline syenite (Wolff *et al.*, 2000). Batch melting models and bulk K_d values were calculated using the average of the modal abundances of six unaltered nepheline syenite samples (Wolff, 1987) and single mineral–melt partition coefficients from Tenerife and other comparable rock suites (Larsen, 1979; Wörner *et al.*, 1983; Nash & Crecraft, 1985; Marks *et al.*, 2004; Olin & Wolff, 2010). The mixing proportions derived from the Sr–Nd isotope modelling were used in the trace element bulk mixing models. Transitional lavas are typically reproduced by uptake of ~33–77% of the assimilated into a mafic melt. The Sr–Nd isotopic fingerprints of the felsic lavas contain 77–99.78% of the felsic component, regardless of whether the composition of a mafic, a transitional or a low $^{87}\text{Sr}/^{86}\text{Sr}$ felsic lava is used as the starting composition. The felsic lava with the highest $^{87}\text{Sr}/^{86}\text{Sr}$ ratio, sample MB7, yields a felsic end-member percentage of >97.8%.

High percentages of the assimilated are thus involved in the mixtures of assimilated and Teide mafic magma. The mixing models reproduce the Teide–Pico Viejo felsic compositions only above a degree of partial melting of $F=0.95$ and best by bulk melting (Fig. 9). It should be noted that the best fit in these calculations is provided by hypothetical melts of a nepheline syenite protolith that is altered. In binary mixing models, bulk or close to bulk crustal melts of altered nepheline syenite are needed to successfully model the compositions of the most extreme felsic Teide lavas. In an AFC scenario, this implies very large degrees of partial melting that approach bulk melting, to be able to produce the most felsic compositions at Teide–Pico Viejo.

Quantification of magmatic differentiation processes at Teide–Pico Viejo

In the preceding discussion, radiogenic and stable isotope data and REE ratios for the Teide–Pico Viejo lavas have

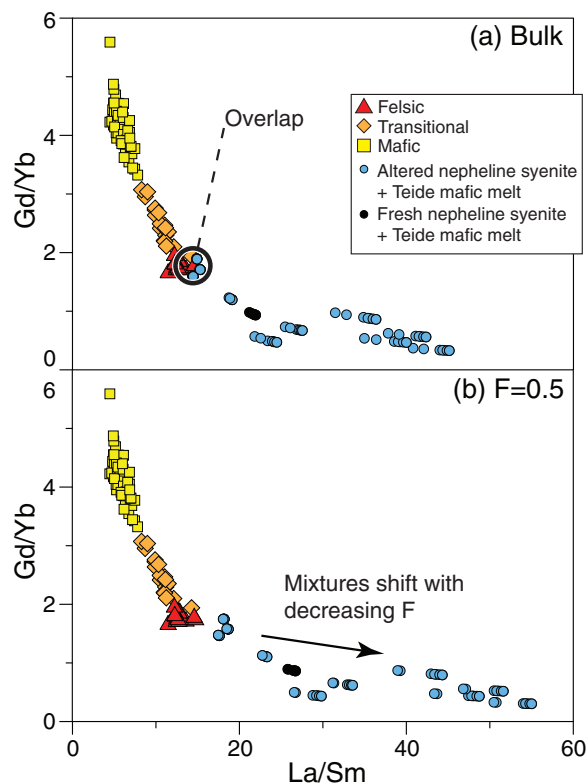


Fig. 9. Gd/Yb vs La/Sm for Teide–Pico Viejo lavas compared with hybrids of nepheline syenite batch partial melts and Teide–Pico Viejo mafic lavas. The degree of partial melting of the Diego Hernández nepheline syenite is indicated. (a) Bulk melting; (b) $F=0.5$.

been used to demonstrate the influence of a highly differentiated igneous assimilated in binary mixing models. Magma mixing has indeed been identified as an important differentiation process in single units in Tenerife (Wiesmaier *et al.*, 2011). However, the binary mixing models presented here have been used to provide qualitative constraints on the characteristics of the assimilated, not to indicate that all differentiation is based on magma mixing. In a magmatic system that involves assimilation of country-rocks, significant amounts of crystallization have to occur (Taylor, 1980). Consequently, the open-system behaviour observed at Teide–Pico Viejo is most probably a result of combined assimilation and fractional crystallization. In the following section, we will attempt to quantify this interplay of fractionation and assimilation at Teide–Pico Viejo.

The EC-AFC model of Spera & Bohrsen (2001) encompasses assimilation and fractional crystallization in a thermodynamic framework and thus permits more realistic assumptions about their intensity and interplay (Spera & Bohrsen, 2001, 2002, 2004). Here, we present an EC-AFC model assuming that one batch of hot, mafic magma thermally equilibrates with surrounding, cooler

nepheline syenite, which produces a highly differentiated assimilated melt of nepheline syenite composition. Teide–Pico Viejo shows little subaerial evidence for hydrothermal alteration and therefore approaches an isenthalpic AFC scenario (see Reiners *et al.*, 1995), for which the EC-AFC model is well suited. The original mafic magma temperature was assumed to be 1200°C ($T_1^m = T_m^0$). We assigned a temperature of 600°C to the Teide–Pico Viejo basement, in agreement with the steep geothermal gradient of 100°C km⁻¹ that has been observed at several kilometres distance from Teide during the drilling project Tenerife I in the 1980s (<http://www.petratherm.com.au/webapp.117699/CanaryIslands>). At the inferred crystallization depths of the felsic magmas of 4–6 km, an elevated temperature of 400–600°C is therefore predicted.

Specific heat capacities and crystallization or fusion enthalpies were calculated from the oxide and mineral values given by Spera & Bohrsen (2001) using the average compositions of the Tenerife Granadilla ignimbrite (Palacz & Wolff, 1989). The equilibration temperature was set at 825°C according to Teide phonolite phase equilibrium experiments (Andújar *et al.*, 2010). The solidus temperature T_s of the nepheline syenite assimilate was set to 700°C (Wolff, 1987). The liquidus temperature T_l^a of the nepheline syenite was assumed to be 820°C based on experimental studies.

Partition coefficients

The closed-system Teide–Pico Viejo model of Ablay *et al.* (1998) provided estimates of the amount of differentiation. Mineral–melt partition coefficients were obtained from Schnetzler & Philpotts (1970), Larsen (1979), Nash & Crecraft (1985), Ewart & Griffin (1994), Marks *et al.* (2004) and Olin & Wolff (2012). To account for progressively changing partition coefficients during differentiation from basalt to phonolite, bulk D_0 values were used in conjunction with enthalpies to create certain variability in the bulk partition coefficients (Spera & Bohrsen, 2001, equations 9A and B).

Assimilant

Because REE ratio models indicate bulk recycling of nepheline syenite, the assimilate's composition in the model is represented by the Nd, Pb, Zr, Hf and Ba composition of Diego Hernández nepheline syenite blocks (Wolff *et al.*, 2000; Table 5). A low Sr/Nd and high ⁸⁷Sr/⁸⁶Sr required by Sr–Nd isotope modelling was combined with a ¹⁴³Nd/¹⁴⁴Nd value of around 0.51294 and ²⁰⁶Pb/²⁰⁴Pb of around 19.78.

EC-AFC results

The normalized mass of melt (M_m) initially drops to about 0.8 (80% of M_0), as crystallization is dominant in the beginning of the simulation. Thereafter, M_m doubles to 1.6 as the production of melt from the wall-rock increases.

The melt productivity of the wall-rock (f_a) reaches unity at T_{eq} (i.e. equivalent to bulk melting of nepheline syenite). The mass of cumulate (M_c) produced approaches unity (i.e. the amount of cumulate almost equals the initial amount of magma intruded). The r value (M_a^*/M_c) is 1.6, reflecting the fact that a greater mass of melt is produced than the mass of crystals solidified and fractionated (see Reiners *et al.*, 1995).

The felsic assimilate and the chosen thermal parameters account adequately well for the geochemical and isotopic variations observed in the Teide–Pico Viejo lavas (Fig. 10). The EC-AFC curves reproduce the entire differentiation sequence in terms of Pb, Zr and Hf compositions. The Sr, Ba and Nd model curves do not, however, reproduce the intermediate compositions. This is an artefact of the EC-AFC calculations, because abrupt changes in bulk compatibility of trace elements are not accounted for in the current state of the code. For example, the bulk partition coefficients of Sr and Ba in the mafic lavas change from incompatible to compatible when plagioclase enters the fractionation sequence. A more incremental approach has been attempted but is not straightforward with the EC-AFC model, because changing starting conditions have to be inferred for each increment, introducing a large potential for error. As a result, in the framework applied here, the EC-AFC code is suitable to model the Sr, Ba and Nd compositions of the mafic and felsic extremes of the Teide–Pico Viejo succession, but not its intermediate members (see Fig. 10). The linear trace element trends of Pb and Hf versus Zr do, however, reproduce the whole range of Teide compositions.

Sr–Nd–Pb isotope ratios are also satisfactorily reproduced. Because the Pb and Nd isotopic ratios are highly variable in the mafic lavas, several different mafic end-member compositions were evaluated (see model curves in Fig. 10). Irrespective of which mafic end-member composition is selected, the models trend towards the same felsic end-member isotope composition during thermal equilibration, thus replicating the naturally occurring trend of isotope compositions. Also, except for one sample, the ⁸⁷Sr/⁸⁶Sr ratios of the Teide succession are well explained by EC-AFC. By and large, the EC-AFC model therefore demonstrates the formation of Teide–Pico Viejo magmas by assimilation of bulk melts of nepheline syenite accompanied by fractional crystallization.

Several features of the EC-AFC model point towards an increase in the amount of assimilation taking place, correlated with the degree of differentiation of the erupted lava. First of all, the batch melting calculations performed using the EC-AFC model require the felsic country rock to be completely melted ($f_a = 1$). The observed increase in r value (M_a^*/M_c) with degree of differentiation confirms that for the more highly differentiated Teide magmas, more bulk melt of the wall-rocks has to be

Table 5: EC-AFC modelling parameters

Thermal parameters						
Liquidus temperature, $T_{l,m}$	1200°C	Crystallization enthalpy, Δh_m (J kg ⁻¹)	398300			
Initial temperature, T_m°	1200°C	Isobaric specific heat of magma, $C_{p,m}$ (J kg ⁻¹ K ⁻¹)	1479			
<i>Assimilant</i>						
Liquidus temperature, $T_{l,a}$	820°C	Fusion enthalpy, Δh_a (J kg ⁻¹)	293500			
Initial temperature, T_a°	600°C	Isobaric specific heat of assimilant, $C_{p,a}$ (J kg ⁻¹ K ⁻¹)	1385			
Solidus temperature, T_s	700°C	Non-linear logistical parameters				
Equilibration temperature, T_{eq}	825°C	Magma a	450			
		Magma b	-10.5			
		Assimilant a	400			
		Assimilant b	-11			
Compositional parameters						
	Sr	Nd	Pb	Zr	Hf	Ba
<i>Pristine magma</i>						
Initial concentration (ppm), C_m°	1200	58	4.09	210	6.39	402
	717.9					
Distribution coefficient, bulk D_0	1.13	0.18	25	0.18	0.38	1×10^{-8}
Enthalpy	-15500	-17500	50000	-10000	-10000	-200000
Isotope ratio, ϵ_m	0.70311	0.512991	19.814159			
		0.512921	19.736138			
		0.512901	19.693148			
$\delta^{18}\text{O}$ ratio (‰)	5.5					
<i>Assimilant</i>						
Initial concentration (ppm), C°	5.89	58	18	1200	25	50
Distribution coefficient, bulk D_0	2.7	0.3	0.7	0.8	0.8	0.1
Enthalpy	-13000	-13000	-2000	-2500	-2500	-13000
Isotope ratio, ϵ_a	0.70570	0.512945	19.781611			
$\delta^{18}\text{O}$ ratio (‰)	6.0					

Pristine magma and assimilant initial and solidus and liquidus temperatures are after literature constraints. Crystallization and fusion enthalpies and isobaric specific heats were computed after Spera & Bohrsen (2001). Non-linear logistical parameters have been set to default values, as recommended by Spera & Bohrsen (2001). Pristine magma trace element concentrations are from Rodríguez-Badiola *et al.* (2006), and isotope ratios from this study. Where a number of end-member compositions have been tested, several values are given. This is reflected in multiple curves in Fig. 11. The assimilant composition was constrained from the isotope modelling and reflects a highly differentiated, alkaline rock.

assimilated. The most differentiated sample, Montaña Blanca (MB7), however, is not replicated by the EC-AFC model, which indicates an even greater amount of assimilant than may have been incorporated. Significant assimilant variability is ruled out based on isotope and trace element constraints. The Sr isotope ratio is therefore a robust indicator of the amount of assimilation. Furthermore, little leeway is permissible in the thermal parameters. Because of this, we speculate that MB7 may be derived by processes additional to combined assimilation and fractional crystallization (e.g. the formation of pure crustal melts).

Potential for crustal melting

The failure of the EC-AFC model to replicate the highest ⁸⁷Sr/⁸⁶Sr sample, Montaña Blanca (MB7), requires a different approach. The EC-AFC model describes the combined effects of wall-rock assimilation and fractional crystallization on a single magma batch. However, when the lack of a common diffusive interface between magma and assimilant precludes the uptake of crustal melt into the resident magma, AFC models are not applicable (see Marshall & Sparks, 1984). In other words, whereas fractional crystallization is necessarily bound to a liquid body of magma, crustal melting may

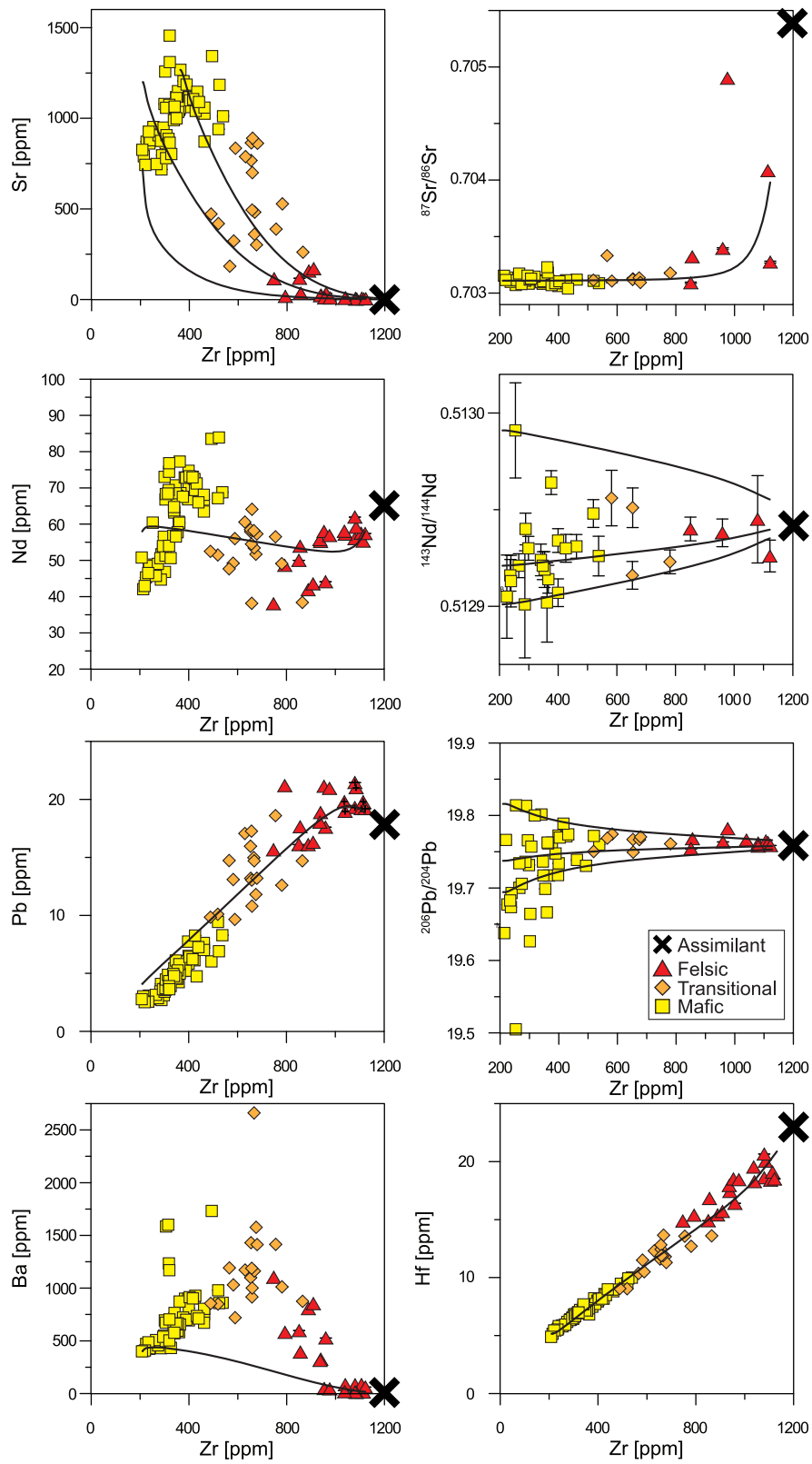


Fig. 10. Results of EC-AFC modelling of the Teide–Pico Viejo succession showing the variation of Sr, Nd, Pb, Zr, Hf and Ba, $^{87}\text{Sr}/^{86}\text{Sr}$, $^{143}\text{Nd}/^{144}\text{Nd}$ and $^{206}\text{Pb}/^{204}\text{Pb}$ vs Zr. Zirconium is used as index of differentiation. Black curves are modelled results; for Nd and Pb isotopes three different starting compositions were used because of the isotopic variability observed in the mafic lavas.

occur in the absence of direct contact with the heat-providing liquid.

In a plot of $^{87}\text{Sr}/^{86}\text{Sr}$ versus $1/^{86}\text{Sr}$, mafic and transitional lavas plot near the origin and are very closely spaced (Fig. 11). The felsic lavas show either high $^{87}\text{Sr}/^{86}\text{Sr}$ ratios or low ^{86}Sr concentrations (high $1/^{86}\text{Sr}$), or a combination of both. The felsic samples RBL-02 and BOQ plot to the right-hand side at high $1/^{86}\text{Sr}$ values. Using the felsic assimilant deduced from isotope and trace element constraints, the model EC-AFC curves reproduce the samples BOQ and RBL-02, but fall short of explaining the Sr isotope composition of sample MB7. Four of the felsic lavas (including Montaña Blanca) define a linear array indicating a mixing relationship with the felsic island core assimilant. Because of the large amount of assimilant in sample MB7 (>98%), this mixing array supports the view that phase 7 of the Montaña Blanca volcano has been formed effectively by crustal melting alone.

The formation of crustal melts largely depends on the conditions during emplacement of mafic magma into the crust; that is, low-solidus country rock material and steep geothermal gradient (Huppert & Sparks, 1988; Annen & Sparks, 2002). In Tenerife, these conditions are met; low-solidus nepheline syenite probably exists at depth and a steep geothermal gradient of $100^\circ\text{C km}^{-1}$ has been observed during earlier drilling operations. The conditions below Teide–Pico Viejo volcano are therefore favourable for melting of appropriate felsic crustal lithologies.

Consistent with rising r values in the EC-AFC model, crustal melting appears to become more dominant in the more highly differentiated rocks of the Teide–Pico Viejo succession. Fractional crystallization, in turn, appears to act more dominantly on the mafic magmas. However, pure crustal melting seems to apply only to a single lava flow in the context of the data presented here (MB7). Because AFC processes or assimilant variability are both insufficient to explain the composition of phase 7 of the Montaña Blanca eruption, we suggest that this lava flow represents more than 98% melting of a pre-Teide nepheline syenite with extremely little juvenile material involved. All other phonolites and less differentiated lavas have been derived from a juvenile, mafic magma by various degrees of assimilation and fractional crystallization.

MODEL

Tenerife is a rather mature volcanic system that has undergone several eruptive cycles, each with a complete suite of alkaline rocks ranging compositionally from mafic to felsic. Within a cycle, eruption frequency appears to decline with degree of differentiation. Teide–Pico Viejo phonolites seldom erupt (about every 1000 years), compared with mafic eruptions that occur 10 times as often (Carracedo *et al.*, 2007).

In the terminal stage of the Las Cañadas volcano (pre-Teide), the highly explosive Diego Hernández phase was accompanied by the Icod landslide, which unroofed the junction of the two active rift zones and probably caused accelerated ascent of magma from depth (see Longpré *et al.*, 2008, 2009). This led to renewed and abundant mafic activity (Carracedo *et al.*, 2007), and the initial, ‘old’ Teide eruptions (~200–100 ka) were consequently basanitic (Rodríguez-Badiola *et al.*, 2006). Evolved intrusive material that corresponds to pre-Teide eruption cycles was not subjected to remelting at this stage, because mafic magmas in the Canary Islands are known to ascend swiftly via dyke systems with little residence time at shallow crustal depths (see Ablay *et al.*, 1998; Rodríguez-Badiola *et al.*, 2006).

Sediment contamination is excluded by the Sr–Pb isotope characteristics of the Teide–Pico Viejo rocks, despite all the magmas having to cross an ~2 km thick sequence of sedimentary oceanic crust (Hoernle, 1998; Ye *et al.*, 1999; Krastel & Schmincke, 2002). Plausibly, pre-existing and shielded magma migration pathways may have been reactivated within the mature Tenerife plumbing system, consistent with rapid magma ascent along dykes from Moho depths. Older lavas may well have experienced a component of sediment assimilation, but this does not appear to have been significant in the Teide–Pico Viejo succession.

The increasing proportion of crustal melt within the more highly differentiated lavas (younger than 15–30 ka) indicates that at some point during the history of Teide–Pico Viejo, the older intrusive rocks began to be recycled to a significant degree, probably triggered by the prolonged residence time of the magma at shallow crustal levels and gradual heating of the wall-rocks. Potential causes for this could be (1) voluminous, landslide-filling layers of fresh, competent basanite caprock erupted from proto-Teide (see Goles, 1976), (2) density filtering owing to the increasing load exerted by the growing Teide–Pico Viejo edifice (see Pinel & Jaupart, 2000) or (3) the formation of density barriers of partially molten, felsic country-rock (Huppert & Sparks, 1988). The resulting underplating would have steepened the geothermal gradient and further reduced the thermal penalty for wholesale melting of the country-rocks (Fig. 12; see Annen & Sparks, 2002).

The onset of crustal melting and melt assimilation must have been progressive, as the transitional lavas erupted at around 30 ka; that is, before the first felsic lavas appeared (Carracedo *et al.*, 2007). These transitional lavas can be expressed geochemically as mixtures of felsic crustal melts and mafic lavas or modelled by AFC processes. The culmination at Teide took place with the eruption of high $^{87}\text{Sr}/^{86}\text{Sr}$ felsic lavas 2000 years ago. According to the results of the EC-AFC modelling, the amount of felsic assimilant in these very recent lavas is predominant.

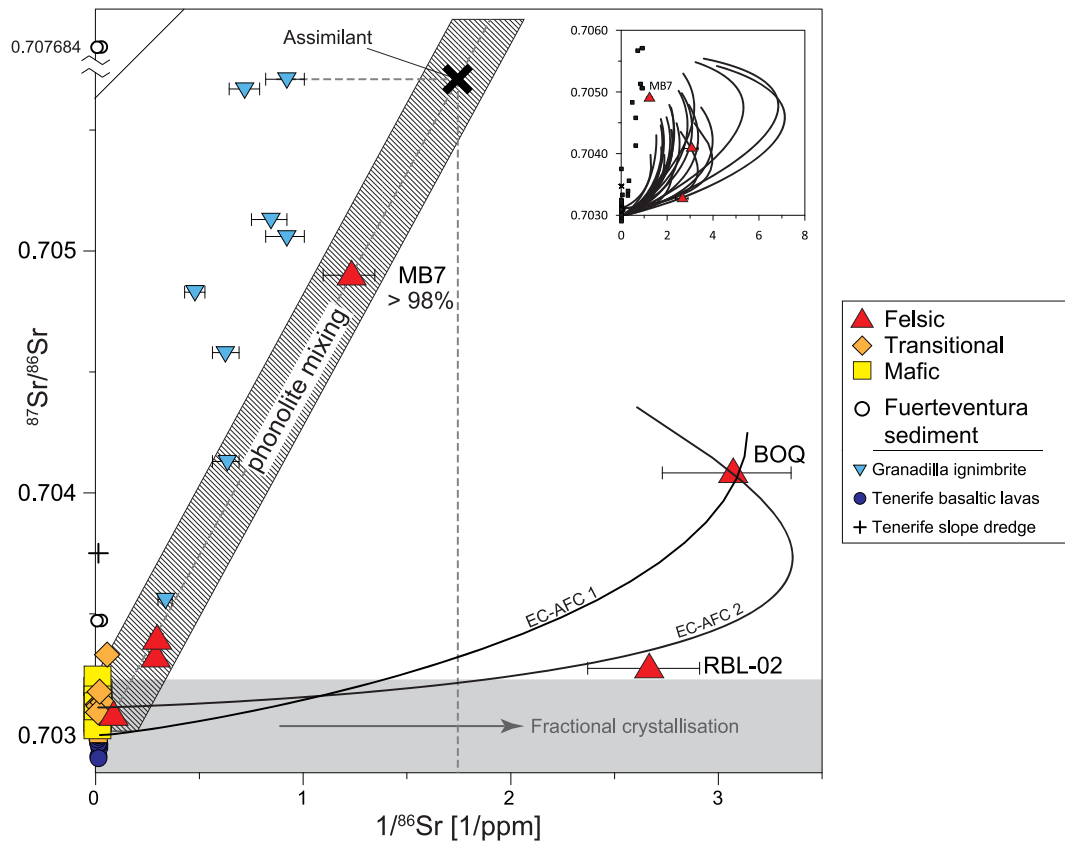


Fig. 11. Groundmass $^{87}\text{Sr}/^{86}\text{Sr}$ vs $1/^{86}\text{Sr}$ for the Teide–Pico Viejo lavas. The concentration of ^{86}Sr is calculated using the measured $^{87}\text{Sr}/^{86}\text{Sr}$ ratio and Sr concentration. The Sr concentration of the assimilant used for EC-AFC modelling was computed to be 5.89 ppm, using Granadilla ignimbrite Sr isotope ratios. The literature data are from Palacz & Wolff (1989), Simonsen *et al.* (2000) and Abratis *et al.* (2002); basaltic lavas and samples dredged from the submarine slopes of Tenerife are precluded as assimilant by their high Sr/Nd ratios and the Fuerteventura sediments show very distinct Pb isotope composition and plot outside the potential mixing array defined by the felsic lavas. Errors (2SD) are contained within the symbol size when invisible. Sr concentrations of Fuerteventura sediments are from F. Deegan (unpublished data). The inset shows various calculated EC-AFC models, all of which are insufficient to model sample MB7 when using the thermal constraints inherent in the Tenerife setting.

This implies that the juvenile magma acted as a heat source at depth to melt the country-rock but remained separated from the newly forming crustal melt (Fig. 12), which formed new and presumably largely isolated pockets of felsic magma.

Crustal melting has been invoked in several tectonic settings to explain the petrogenesis of felsic magmas (e.g. Flagler & Spray, 1991; Sawyer, 1991; Troll *et al.*, 2004, 2005; Ferla & Meli, 2006). For ocean islands, in particular, a number of workers have argued for this mode of felsic magma generation (e.g. Williams *et al.*, 1995; Bohrson & Reid, 1998; Borg & Clyne, 1998; Troll & Schmincke, 2002). Legendre *et al.* (2005) suggested a large variety of differentiation processes for the alkaline magma series of Ua Pou Island (French Polynesia); these included a crustal melt origin for the compositionally most extreme phonolites, very similar to our inferences for Teide–Pico Viejo. In comparison with the east African rift valley, Tenerife shows a much simplified crustal structure, which narrows

down assimilant variability. Somewhat arbitrarily, Baker (1987) dismissed a crustal melting influence in the east African phonolites because of a lack of correlation of Rb/Sr with $^{87}\text{Sr}/^{86}\text{Sr}$ in these rocks. At Teide–Pico Viejo such a correlation is lacking, too, yet the isotope evidence for a crustal component is unequivocal. High-pressure phase relation experiments conducted on Kenyan plateau phonolites have provided evidence for deep crustal equilibration, requiring a combination of fractional crystallization and assimilation of partial melts from a basaltic protolith, facilitated by increased conductive heat flow from the injected or underplated magma (Hay & Wendlandt, 1995).

A very similar mechanism to the one invoked here might have involved recycled crust earlier in the evolution of Tenerife. Isotope data for the pre-Teide Las Cañadas phonolites led Wolff & Palacz (1989) to suggest ‘that the contaminant be present within the volcanic pile itself’, thus underlining self-recycling as a relevant process in Tenerife.

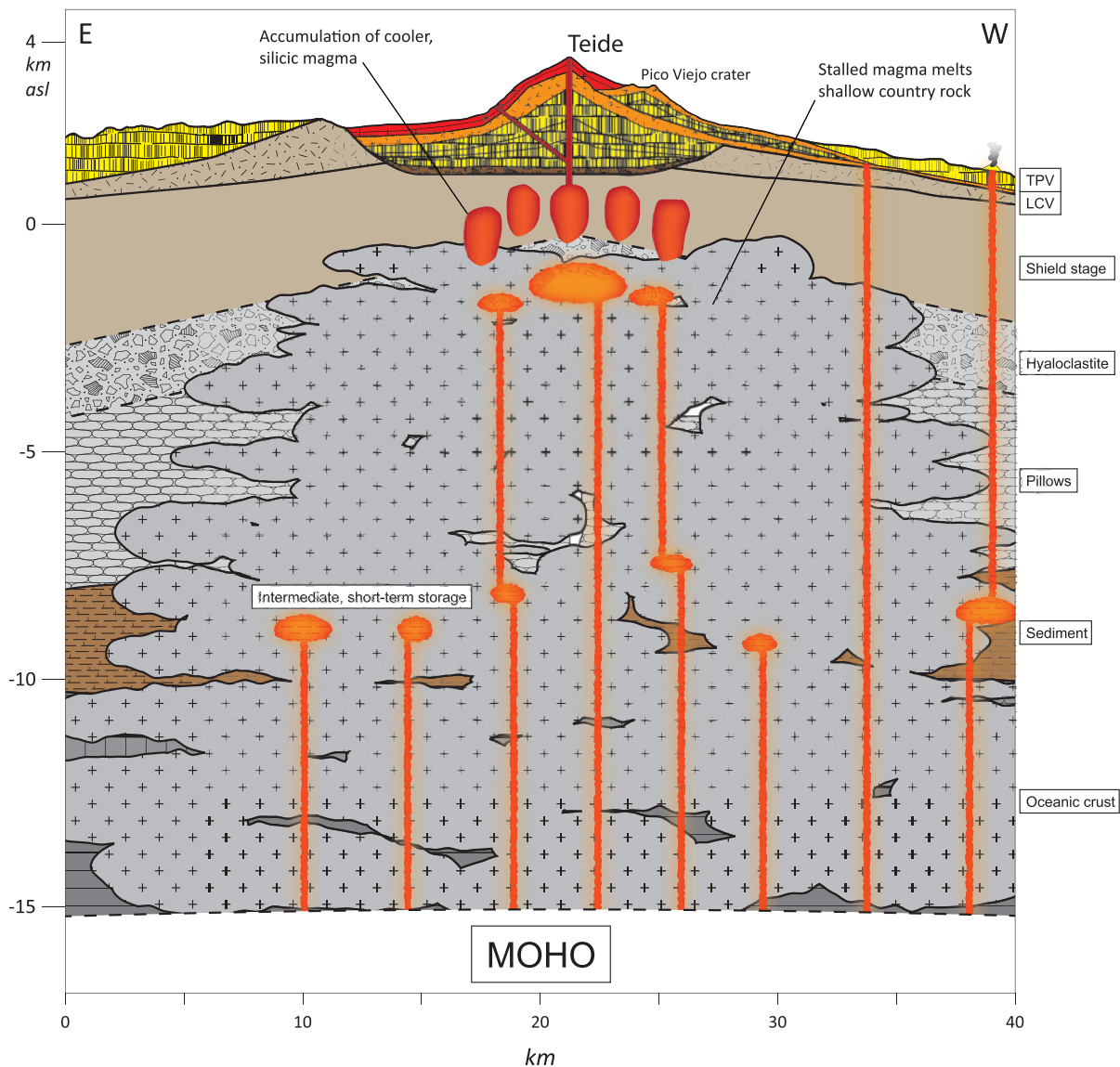


Fig. 12. Interpretation of the east–west cross-section of the current plumbing system of Tenerife (1.8 × vertical exaggeration). Deep island core and ocean crust lithology are represented in this sketch for orientation but may in fact have been largely reworked by Tenerife’s igneous activity since Miocene times. Included is information from the following publications: crustal structure, Krastel *et al.* (2002); seamount sequence, Staudigel & Schmincke (1984); Teide–Pico Viejo and underlying units, Carracedo *et al.* (2007); height of landslide breccia, Márquez *et al.* (2008); inverse geothermal gradient, Annen & Sparks (2002). Lower crust–upper mantle as the main crystallization level has been invoked by several workers (e.g. Ablay *et al.*, 1998; Hill *et al.*, 2002; Spera & Bohron, 2004). In the Canary Islands specifically, intermediate levels of short-term residence of magma were detected, inferred from the re-equilibration of CO₂ inclusions in mineral phases (Klügel *et al.*, 2005; Galipp *et al.*, 2006; Longpré *et al.*, 2008). Underplating of hot, mafic material underneath the central Teide–Pico Viejo complex may cause the formation of crustal melt pockets, decoupled from the heat-providing juvenile material. LCV, Las Cañadas volcano.

Implications for ocean island magmatic differentiation

One of the most puzzling questions in the history of magmatic differentiation has been the overabundance of highly evolved compositions compared with intermediate

magmas. Why should this occur in a system where fractionation of phenocryst phases is thought to continuously drive magma from low to high silica concentrations? Several aspects are inconsistent with a pure fractionation-driven processes. First of all, closed-system fractionation

models fail convincingly and systematically to explain all the trace element variations. Second, in the TAS diagram, the felsic Teide lavas form an array at a steep angle to the main liquid line of descent. Figure 6 of Ablay *et al.* (1998) shows the same sub-vertical trend in a plot of Na₂O versus SiO₂. Such trends are usually interpreted as being controlled by partial melting and assimilation (see Mollo *et al.*, 2010). Third, the trend of the felsic lavas is completely engulfed by data for Tenerife nepheline syenite and ignimbrite compositions (Palacz & Wolff, 1989; Wolff *et al.*, 2000), the types of highly differentiated rocks that are the likely protoliths for assimilation or crustal melting at Teide–Pico Viejo. Classifying the Teide lavas based on their sub-parallel trace element patterns allowed lavas of similar geochemical history to be distinguished and the sub-vertical trend in the alkali contents of the felsic lavas to be recognized. We therefore suggest that for differentiation sequences in a single volcanic setting, grouping of the erupted deposits based on their trace element patterns should be attempted. These first-order constraints allow the grouping of deposits with broadly comparable magmatic histories. Interpretations of trends in major and trace element chemistry can thus be interpreted firmly grounded on the characteristics inherent in a single volcanic setting.

In contrast, pockets of crustal melt that form spatially disconnected from the juvenile magma bodies can explain several characteristics of Teide–Pico Viejo in a much simpler way.

- (1) The bimodality, both in number and volume, of the erupted compositions is better explained when the formation of crustal melts is spatially disconnected from the juvenile mafic material. An overabundance of highly differentiated lavas may be caused by reworking highly differentiated country-rocks or by partially melting mafic protoliths (see Hay & Wendlandt, 1995; Hay *et al.*, 1995; Price *et al.*, 2003). In this scenario, the paucity of erupted intermediate compositions is an artefact of the two principal processes, fractionation and crustal melting, which act from both ends of the SiO₂ spectrum. Crustal melting is perhaps more prevalent in settings where protoliths of low solidus temperature are available for melting. In ocean islands, highly differentiated material is present as a potential assimilated from the earliest stages of island evolution. Staudigel & Schmincke (1984) documented trachytes in the seamount sequence of La Palma, and in Tenerife there are phonolite plugs of 6 Ma minimum age within the earliest shield-building stages (Carracedo, 1979; Walter *et al.*, 2005; Longpré *et al.*, 2009). At later times, even larger volumes of felsic magma were produced in Tenerife, which, combined with the fact that sediment assimilation plays no role here, may make Teide–Pico Viejo a setting
- (2) Self-recycling of the island edifice allows for rapid formation of felsic magma. Previously thought to take up to 300 kyr in Tenerife (Hawkesworth *et al.*, 2000), the generation of felsic magma by crustal melting is probably achieved on much faster timescales. Huppert & Sparks (1988), for example, suggested a period of 10²–10³ years for roof melting and formation of a felsic cupola above large magma chambers. Such a timescale approaches the observed frequency of phonolite eruptions at Teide (once every 1000 years) and is consistent with the notion of multiple, shallow magma reservoirs below Teide (e.g. Triebold *et al.*, 2006; Martí & Geyer, 2009).
- (3) Tenerife phonolite lavas show much larger eruption volumes than the mafic lavas, by 2–3 orders of magnitude (Carracedo *et al.*, 2008). Closed-system fractional crystallization would require very large degrees of fractionation to form the felsic magma (>88% in Tenerife; Ablay *et al.*, 1998) and the resulting cumulate rocks would be difficult to accommodate within the magmatic plumbing system (see O'Hara, 1998). Self-recycling provides a mechanism to emplace magma within a volcanic edifice without the need to accommodate unreasonably large volumes of cumulates. Crustal recycling has also been invoked for large-volume silicic eruptions elsewhere; for example, along the Yellowstone hotspot track where crustal δ¹⁸O signatures in rhyolites correlate with eruption volumes (Watts *et al.*, 2011), or the extremely radiogenic felsic ignimbrites associated with the mafic Rum igneous centre in Scotland (Troll *et al.*, 2004, 2008).

CONCLUSIONS

The Sr, Nd, Pb and O isotope data presented here allow a coherent model of combined assimilation and fractional crystallization to be devised to explain the origin of the Teide–Pico Viejo succession in Tenerife. The end-member components in the model are (1) mafic Teide magmas of uniform, unradiogenic Sr and variable Nd and Pb isotope composition and (2) a felsic crustal component with high ⁸⁷Sr/⁸⁶Sr and uniform Nd and Pb (but variable oxygen) isotope composition that we argue is a melt formed from older felsic intrusive rocks.

The Sr and Pb isotope data show that the Teide–Pico Viejo succession is the product of an open system, but preclude significant oceanic sediment contamination. The Sr isotope data indicate that a component with high $^{87}\text{Sr}/^{86}\text{Sr}$ must be involved in the evolution of the magmas within the plumbing system. In Tenerife, such high $^{87}\text{Sr}/^{86}\text{Sr}$ ratios are rare and restricted to highly differentiated igneous rocks. Furthermore, isotope and EC-AFC modelling require involvement of a component with low Sr/Nd, low Sr concentration, high concentrations of incompatible elements, restricted $^{143}\text{Nd}/^{144}\text{Nd}$ and $^{206}\text{Pb}/^{204}\text{Pb}$, and extremely low $^{207}\text{Pb}/^{204}\text{Pb}$. This is most likely to be a highly differentiated igneous rock or a melt derived therefrom. Additionally, oxygen isotope compositions for Teide–Pico Viejo feldspar and groundmass separates vary between eruptions, meaning that the high $^{87}\text{Sr}/^{86}\text{Sr}$ component has variable $\delta^{18}\text{O}$. Nepheline syenite lithic blocks from pre-Teide ignimbrites have the geochemical characteristics expected of the high $^{87}\text{Sr}/^{86}\text{Sr}$ component and are likely to represent the intrusive material that is abundant below Teide–Pico Viejo. The variability in $\delta^{18}\text{O}$ suggests that the nepheline syenites at depth vary from fresh to hydrothermally altered (lower and higher $\delta^{18}\text{O}$ than normal). The REE compositions of altered nepheline syenite are a close fit to the abundances predicted for the felsic high $^{87}\text{Sr}/^{86}\text{Sr}$ component involved in the AFC process. In the formation of the compositionally most extreme phonolite magma at Teide–Pico Viejo, crustal melts are dominant. Constraints from Sr–Nd isotope modelling indicate that large amounts of a recycled crustal component (>98%) make up the most radiogenic phonolite, Montaña Blanca phase 7. Using thermal constraints corroborated by drilling and phase equilibrium data, EC-AFC modelling cannot reproduce the composition of this Montaña Blanca phonolite. This phonolite, however, plots on a mixing array between mafic lavas and a felsic crustal assimilated. Because other end-members or variability in the felsic component are ruled out, we invoke the formation of an independent pocket of felsic crustal melt for phase 7 of the Montaña Blanca phonolite.

Compositional bimodality has been demonstrated to exist in the case of Teide–Pico Viejo. Almost all lavas types have been sampled, and have been sampled only once to avoid over-representation of any type of lava. The most primitive magma compositions evolve towards intermediate compositions mainly by means of fractional crystallization and variable but small degrees of wall-rock assimilation. In turn, the highly differentiated magmas may form by AFC processes or, in special cases, by partial or wholesale melting of felsic country-rocks. The observed contrast in differentiation processes between the mafic and felsic lavas explains the bimodality of the erupted lavas in the Teide–Pico Viejo succession and thus provides a straightforward and consistent model for the Bunsen–Daly Gap in Tenerife.

ACKNOWLEDGEMENTS

Richard C. Price, John C. White and an anonymous reviewer are greatly thanked for constructive reviews of the paper. G. Wörner is thanked for his thoughtful and thorough review of an earlier version of the paper. Anne Kelly and Vinnie Gallagher at the Scottish Universities Environmental Research Centre, East Kilbride, Scotland, UK greatly helped with clean laboratory procedures and radiogenic isotope analyses.

FUNDING

S.W. and V.R.T. acknowledge support from the School of Natural Sciences at Trinity College Dublin and Science Foundation Ireland (SFI), V.R.T. from the faculty of Technology and Natural Sciences (TekNat) at Uppsala University, and I.N.B. from National Science Foundation (NSF) grant EAR0844772.

REFERENCES

- Abdel-Monem, A., Watkins, N. D. & Gast, P. W. (1971). Potassium–argon ages, volcanic stratigraphy, and geomagnetic polarity history of the Canary Islands; Lanzarote, Fuerteventura, Gran Canaria, and La Gomera. *American Journal of Science* **271**, 490–521.
- Abdel-Monem, A., Watkins, N. D. & Gast, P. W. (1972). Potassium–argon ages, volcanic stratigraphy, and geomagnetic polarity history of the Canary Islands; Tenerife, La Palma and Hierro. *American Journal of Science* **272**, 805–825.
- Ablay, G. J., Carroll, M. R., Palmer, M. R., Martí, J. & Sparks, R. S. J. (1998). Basanite–phonolite lineages of the Teide–Pico Viejo volcanic complex, Tenerife, Canary Islands. *Journal of Petrology* **39**, 905–936.
- Abratis, M., Schmincke, H. U. & Hansteen, T. (2002). Composition and evolution of submarine volcanic rocks from the central and western Canary Islands. *International Journal of Earth Sciences* **91**, 562–582.
- Adam, J. & Green, T. (2006). Trace element partitioning between mica- and amphibole-bearing garnet lherzolite and hydrous basanitic melt: 1. Experimental results and the investigation of controls on partitioning behaviour. *Contributions to Mineralogy and Petrology* **152**, 1–17.
- Ancochea, E., Fuster, J., Ibarrola, E., Cendrero, A., Coello, J., Hernan, F., Cantagrel, J. M. & Jamond, C. (1990). Volcanic evolution of the island of Tenerife (Canary Islands) in the light of new K–Ar data. *Journal of Volcanology and Geothermal Research* **44**, 231–249.
- Ancochea, E., Huertas, M. J., Cantagrel, J. M., Coello, J., Fuster, J. M., Arnaud, N. & Ibarrola, E. (1999). Evolution of the Canadas edifice and its implications for the origin of the Canadas Caldera (Tenerife, Canary Islands). *Journal of Volcanology and Geothermal Research* **88**, 177–199.
- Andújar, J., Costa, F. & Martí, J. (2010). Magma storage conditions of the last eruption of Teide volcano (Canary Islands, Spain). *Bulletin of Volcanology* **72**, 381–395.
- Anguita, F. & Hernán, F. (2000). The Canary Islands origin: a unifying model. *Journal of Volcanology and Geothermal Research* **103**, 1–26.
- Annen, C. & Sparks, R. S. J. (2002). Effects of repetitive emplacement of basaltic intrusions on thermal evolution and melt generation in the crust. *Earth and Planetary Science Letters* **203**, 937–955.

- Araña, V., Martí, J., Aparicio, A., García-Cacho, L. & García-García, R. (1994). Magma mixing in alkaline magmas: An example from Tenerife, Canary Islands. *Lithos* **32**, 1–19.
- Bailey, D. K. (1987). Mantle metasomatism—perspective and prospect. In: Fitton, J. G. & Upton, B. G. J. (eds) *Alkaline Igneous Rocks*. Geological Society, London: Special Publications **30**, 1–13.
- Baker, B. H. (1987). Outline of the petrology of the Kenya rift alkaline province. In: Fitton, J. G. & Upton, B. G. J. (eds) *Alkaline Igneous Rocks*. Geological Society, London: Special Publications **30**, 293–311.
- Baker, B. H., Williams, L. A. J., Miller, J. A. & Fitch, F. J. (1971). Sequence and geochronology of the Kenya rift volcanics. *Tectonophysics* **11**, 191–215.
- Baker, I. (1968). Intermediate oceanic volcanic rocks and the ‘Daly gap’. *Earth and Planetary Science Letters* **4**, 103–106.
- Barth, T. F. W., Correns, C. W. & Eskola, P. (1939). *Die Entstehung der Gesteine*. Berlin: Springer.
- Belshaw, N. S., Freedman, P. A., O’Nions, R. K., Frank, M. & Guo, Y. (1998). A new variable dispersion double-focusing plasma mass spectrometer with performance illustrated for Pb isotopes. *International Journal of Mass Spectrometry* **181**, 51–58.
- Bindeman, I. N. (2008). Oxygen isotopes in mantle and crustal magmas as revealed by single crystal analysis. In: Putirka, K. D. & Tepley, F. J., III (eds) *Minerals, Inclusions and Volcanic Processes*. Mineralogical Society of America and Geochemical Society, *Reviews in Mineralogy and Geochemistry* **69**, 445–478.
- Bindeman, I. N., Ponomareva, V. V., Bailey, J. C. & Valley, J. W. (2004). Volcanic arc of Kamchatka: a province with high- $\delta^{18}\text{O}$ magma sources and large-scale $^{18}\text{O}/^{16}\text{O}$ depletion of the upper crust. *Geochimica et Cosmochimica Acta* **68**, 841–865.
- Bohrson, W. A. & Reid, M. R. (1998). Genesis of evolved ocean island magmas by deep- and shallow-level basement recycling, Socorro Island, Mexico: constraints from Th and other isotope signatures. *Journal of Petrology* **39**, 995–1008.
- Bonnefoi, C. C., Provost, A. & Albarède, F. (1995). The ‘Daly gap’ as a magmatic catastrophe. *Nature* **378**, 270–272.
- Borg, L. E. & Clyne, M. A. (1998). The petrogenesis of felsic calc-alkaline magmas from the southernmost Cascades, California: origin by partial melting of basaltic lower crust. *Journal of Petrology* **39**, 1197–1222.
- Brophy, J. G. (1991). Composition gaps, critical crystallinity, and fractional crystallization in orogenic (calc-alkaline) magmatic systems. *Contributions to Mineralogy and Petrology* **109**, 173–182.
- Brown, R. J. & Branney, M. J. (2004). Event-stratigraphy of a caldera-forming ignimbrite eruption on Tenerife: the 273 ka Poris Formation. *Bulletin of Volcanology* **66**, 392–416.
- Brown, R. J., Barry, T. L., Branney, J. J., Pringle, M. S. & Bryan, S. E. (2003). The Quaternary pyroclastic succession of Southeast Tenerife, Canary Islands; explosive eruptions, related caldera subsidence, and sector collapse. *Geological Magazine* **140**, 265–288.
- Bryan, S. E., Martí, J. & Cas, R. A. F. (1998). Stratigraphy of the Bandas del Sur Formation: an extracaldera record of Quaternary phonolitic explosive eruptions from the Las Canadas edifice, Tenerife (Canary Islands). *Geological Magazine* **135**, 605–636.
- Bryan, S. E., Cas, R. A. F. & Martí, J. (2000). The 0–57 Ma plinian eruption of the Granadilla Member, Tenerife (Canary Islands): an example of complexity in eruption dynamics and evolution. *Journal of Volcanology and Geothermal Research* **103**, 209–238.
- Bunsen, R. (1851). Ueber die Prozesse der vulkanischen Gesteinsbildungen Islands. *Annalen der Physik und Chemie* **159**, 197–272.
- Cann, J. R. (1968). Bimodal distribution of rocks from volcanic islands. *Earth and Planetary Science Letters* **4**, 479–480.
- Carracedo, J. C. (1979). *Paleomagnetismo y historia geológica de Tenerife*, Santa Cruz de Tenerife: Aula Cultura Cabildo Insular de Tenerife.
- Carracedo, J. C. (1994). The Canary Islands: An example of structural control on the growth of large oceanic-island volcanoes. *Journal of Volcanology and Geothermal Research* **60**, 225–241.
- Carracedo, J. C. (1996). Morphological and structural evolution of the western Canary Islands: hotspot-induced three-armed rifts or regional tectonic trends? *Journal of Volcanology and Geothermal Research* **72**, 151–162.
- Carracedo, J. C. (1999). Growth, structure, instability and collapse of Canarian volcanoes and comparisons with Hawaiian volcanoes. *Journal of Volcanology and Geothermal Research* **94**, 1–19.
- Carracedo, J. C., Rodríguez Badiola, E., Guillou, H., Paterne, M., Scaillet, S., Pérez Torrado, F. J., Paris, R., Fra-Paleo, U. & Hansen, A. (2007). Eruptive and structural history of Teide volcano and rift zones of Tenerife, Canary Islands. *Geological Society of America Bulletin* **119**, 1027–1051.
- Carracedo, J. C., Rodríguez Badiola, E., Guillou, H., Paterne, M., Scaillet, S., Pérez Torrado, F. J., Paris, R., Rodríguez González, A. & Socorro, S. (2008). *El Volcán Teide—Volcanología, Interpretación de Pasajes y Itinerarios Comentados*. Caja General de Ahorros de Canarias.
- Carracedo, J.-C., Guillou, H., Nomade, S., Rodríguez-Badiola, E., Pérez Torrado, F. J., Rodríguez González, A., Paris, R., Troll, V. R., Wiesmaier, S., Delcamp, A. & Fernandez-Turiel, J. L. (2010). Evolution of ocean island rifts: the Northeast rift zone of Tenerife, Canary Islands. *Geological Society of America Bulletin* **123**, 562–584.
- Chayes, F. (1963). Relative abundance of intermediate members of the oceanic basalt–trachyte association. *Journal of Geophysical Research* **68**, 1519–1535.
- Chayes, F. (1977). The oceanic basalt–trachyte relation in general and in the Canary Islands. *American Mineralogist* **62**, 666–671.
- Christensen, J. N. & DePaolo, D. J. (1993). Time scales of large volume silicic magma systems: Sr isotopic systematics of phenocrysts and glass from the Bishop Tuff, Long Valley, California. *Contributions to Mineralogy and Petrology* **113**, 100–114.
- Clague, D. A. (1978). The oceanic basalt–trachyte association: an explanation of the Daly Gap. *Journal of Geology* **86**, 739–743.
- Daly, R. A. (1925). The geology of Ascension Island. *Proceedings of the American Academy of Arts and Sciences* **60**, 3–80.
- Duncan, R. A. (1981). Hotspots in the southern oceans, an absolute frame of reference for the motion of the Gondwana continents. *Tectonophysics* **74**, 29–42.
- Edgar, C. J., Wolff, J. A., Nichols, H. J., Cas, R. A. F. & Martí, J. (2002). A complex Quaternary ignimbrite-forming phonolitic eruption: the Poris Member of the Diego Hernández Formation (Tenerife, Canary Islands). *Journal of Volcanology and Geothermal Research* **118**, 99–130.
- Edgar, C. J., Wolff, J. A., Olin, P. H., Nichols, H. J., Pittari, A., Cas, R. A. F., Reiners, P. W., Spell, T. L. & Martí, J. (2007). The late Quaternary Diego Hernandez Formation, Tenerife: Volcanology of a complex cycle of voluminous explosive phonolitic eruptions. *Journal of Volcanology and Geothermal Research* **160**, 59–85.
- Ellam, R. M. (2006). New constraints on the petrogenesis of the Nuanetsi picrite basalts from Pb and Hf isotope data. *Earth and Planetary Science Letters* **245**, 153–161.
- Ewart, A. & Griffin, W. L. (1994). Application of proton-microprobe data to trace-element partitioning in volcanic rocks. *Chemical Geology* **117**, 251–284.
- Ferla, P. & Meli, C. (2006). Evidence of magma mixing in the ‘Daly Gap’ of alkaline suites: a case study from the enclaves of Pantelleria (Italy). *Journal of Petrology* **47**, 1467–1507.
- Flagler, P. A. & Spray, J. G. (1991). Generation of plagiogranite by amphibolite anatexis in oceanic shear zones. *Geology* **19**, 70–73.

- Füster, J. M., Cendrero, A., Gastesi, P., Ibarrola, E. & López Ruiz, J. (1968). *Geology and Volcanology of the Canary Islands, Fuerteventura*. Madrid: Instituto Lucas Mallada.
- Galipp, K., Klügel, A. & Hansteen, T. H. (2006). Changing depths of magma fractionation and stagnation during the evolution of an oceanic island volcano: La Palma (Canary Islands). *Journal of Volcanology and Geothermal Research* **155**, 285–306.
- Garcia, M. O., Frey, F. A. & Grooms, D. G. (1986). Petrology of volcanic rocks from Kaula Island, Hawaii. *Contributions to Mineralogy and Petrology* **94**, 461–471.
- Garcia, M. O., Ito, E., Eiler, J. M. & Pietruszka, A. J. (1998). Crustal contamination of Kilauea volcano magmas revealed by oxygen isotope analyses of glass and olivine from Puu Oo eruption lavas. *Journal of Petrology* **39**, 803–817.
- Geldmacher, J., Hoernle, K., Hanan, B., Blichert-Toft, J., Hauff, F., Gill, J. & Schmincke, H.-U. (2011). Hafnium isotopic variations in East Atlantic intraplate volcanism. *Contributions to Mineralogy and Petrology* **162**, 21–36.
- Goles, G. G. (1976). Some constraints on the origin of phonolites from the Gregory Rift, Kenya, and inferences concerning basaltic magmas in the Rift System. *Lithos* **9**, 1–8.
- Guillou, H., Carracedo, J. C., Paris, R. & Perez Torrado, F. J. (2004). Implications for the early shield-stage evolution of Tenerife from K/Ar ages and magnetic stratigraphy. *Earth and Planetary Science Letters* **222**, 599–614.
- Gurenko, A. A., Hoernle, K. A., Hauff, F., Schmincke, H. U., Han, D., Miura, Y. N. & Kaneoka, I. (2006). Major, trace element and Nd–Sr–Pb–O–He–Ar isotope signatures of shield stage lavas from the central and western Canary Islands: Insights into mantle and crustal processes. *Chemical Geology* **233**, 75–112.
- Halliday, A. N., Mahood, G. A., Holden, P., Metz, J. M., Dempster, T. J. & Davidson, J. P. (1989). Evidence for long residence times of rhyolitic magma in the Long Valley magmatic system: the isotopic record in precaldera lavas of Glass Mountain. *Earth and Planetary Science Letters* **94**, 274–290.
- Hansteen, T. H. & Troll, V. R. (2003). Oxygen isotope composition of xenoliths from the oceanic crust and volcanic edifice beneath Gran Canaria (Canary Islands): consequences for crustal contamination of ascending magmas. *Chemical Geology* **193**, 181–193.
- Harris, C., Smith, H. S. & le Roex, A. P. (2000). Oxygen isotope composition of phenocrysts from Tristan da Cunha and Gough Island lavas: variation with fractional crystallization and evidence for assimilation. *Contributions to Mineralogy and Petrology* **138**, 164–175.
- Harris, P. G. (1963). Comments on a paper by F. Chayes, 'Relative abundance of intermediate members of the oceanic basalt–trachyte association'. *Journal of Geophysical Research* **68**, 5103–5107.
- Hart, S. R. (1984). A large-scale isotope anomaly in the Southern Hemisphere mantle. *Nature* **309**, 753–757.
- Hawkesworth, C. J., Blake, S., Evans, P., Hughes, R., Macdonald, R., Thomas, L. E., Turner, S. P. & Zellmer, G. (2000). Time scales of crystal fractionation in magma chambers—integrating physical, isotopic and geochemical perspectives. *Journal of Petrology* **41**, 991–1006.
- Hay, D. E. & Wendlandt, R. F. (1995). The origin of Kenya rift plateau-type flood phonolites: Results of high-pressure/high-temperature experiments in the systems phonolite–H₂O and phonolite–H₂O–CO₂. *Journal of Geophysical Research* **100**, 401–410.
- Hay, D. E., Wendlandt, R. F. & Wendlandt, E. D. (1995). The origin of Kenya rift plateau-type flood phonolites: Evidence from geochemical studies for fusion of lower crust modified by alkali basaltic magmatism. *Journal of Geophysical Research* **100**, 411–422.
- Hill, D. P., Pollitz, F. & Newhall, C. (2002). Earthquake–volcano interactions. *Physics Today* November **2002**, 41–47.
- Hobson, A., Bussy, F. & Hernandez, J. (1998). Shallow-level migmatization of gabbros in a metamorphic contact aureole, Fuerteventura Basal Complex, Canary Islands. *Journal of Petrology* **39**, 1025–1037.
- Hoernle, K. (1998). Geochemistry of Jurassic oceanic crust beneath Gran Canaria (Canary Islands): implications for crustal recycling and assimilation. *Journal of Petrology* **39**, 859–880.
- Hoernle, K., Tilton, G. & Schmincke, H.-U. (1991). Sr–Nd–Pb isotopic evolution of Gran Canaria: Evidence for shallow enriched mantle beneath the Canary Islands. *Earth and Planetary Science Letters* **106**, 44–63.
- Hoernle, K. A. & Schmincke, H.-U. (1993). The role of partial melting in the 15-Ma geochemical evolution of Gran Canaria: a blob model for the Canarian hotspot. *Journal of Petrology* **34**, 599–626.
- Huppert, H. E. & Sparks, R. S. J. (1988). The generation of granitic magmas by intrusion of basalt into continental crust. *Journal of Petrology* **29**, 599–624.
- Klitgord, K. D. & Schouten, H. (1986). Plate kinematics of the Central Atlantic. In: Vogt, P. R. & Tucholke, B. E. (eds) *Geological Society of America, The Geology of North America: the Western Atlantic Region Volume M*, 351–378.
- Klügel, A., Hansteen, T. H. & Galipp, K. (2005). Magma storage and underplating beneath Cumbre Vieja volcano, La Palma (Canary Islands). *Earth and Planetary Science Letters* **236**, 211–226.
- Krastel, S. & Schmincke, H.-U. (2002). Crustal structure of northern Gran Canaria, Canary Islands, deduced from active seismic tomography. *Journal of Volcanology and Geothermal Research* **115**, 153–177.
- Larsen, L. M. (1979). Distribution of REE and other trace elements between phenocrysts and peralkaline undersaturated magmas, exemplified by rocks from the Gardar igneous province, south Greenland. *Lithos* **12**, 303–315.
- Le Bas, M. J., Maitre, R. W. L., Streckeisen, A., Zanettin, B. & IUGS Subcommission on the Systematics of Igneous Rocks (1986). A chemical classification of volcanic rocks based on the total alkali–silica diagram. *Journal of Petrology* **27**, 745–750.
- Legendre, C., Maury, R. C., Caroff, M., Guillou, H., Cotten, J., Chauvel, C., Bollinger, C., Hemond, C., Guille, G., Blais, S., Rossi, P. & Savanier, D. (2005). Origin of exceptionally abundant phonolites on Ua Pou Island (Marquesas, French Polynesia): partial melting of basanites followed by crustal contamination. *Journal of Petrology* **46**, 1925–1962.
- Lemarchand, F., Villemant, B. & Calas, G. (1987). Trace element distribution coefficients in alkaline series. *Geochimica et Cosmochimica Acta* **51**, 1071–1081.
- Lippard, S. J. (1973). The petrology of phonolites from the Kenya Rift. *Lithos* **6**, 217–234.
- Longpré, M.-A., Troll, V. R. & Hansteen, T. H. (2008). Upper mantle magma storage and transport under a Canarian shield-volcano, Teno, Tenerife (Spain). *Journal of Geophysical Research* **113**, B08203.
- Longpré, M.-A., Troll, V. R., Walter, T. R. & Hansteen, T. H. (2009). Volcanic and geochemical evolution of the Teno massif, Tenerife, Canary Islands: Some repercussions of giant landslides on ocean island magmatism. *Geochemistry, Geophysics, Geosystems* **10**, Q12017.
- Marks, M., Halama, R., Wenzel, T. & Markl, G. (2004). Trace element variations in clinopyroxene and amphibole from alkaline to peralkaline syenites and granites: implications for mineral–melt trace-element partitioning. *Chemical Geology* **211**, 185–215.
- Márquez, A., López, I., Herrera, R., Martín-González, F., Izquierdo, T. & Carreño, F. (2008). Spreading and potential instability of Teide volcano, Tenerife, Canary Islands. *Geophysical Research Letters* **35**, doi:10.1029/2007GL032625.
- Marsh, B. D. (1981). On the crystallinity, probability of occurrence, and rheology of lava and magma. *Contributions to Mineralogy and Petrology* **78**, 85–98.

- Marshall, L. A. & Sparks, R. S. J. (1984). Origin of some mixed-magma and net-veined ring intrusions. *Journal of the Geological Society, London* **141**, 171–182.
- Martí, J. & Geyer, A. (2009). Central vs flank eruptions at Teide–Pico Viejo twin stratovolcanoes (Tenerife, Canary Islands). *Journal of Volcanology and Geothermal Research* **181**, 47–60.
- Martí, J. & Gudmundsson, A. (2000). The Las Cañadas caldera (Tenerife, Canary Islands): an overlapping collapse caldera generated by magma-chamber migration. *Journal of Volcanology and Geothermal Research* **103**, 161–173.
- Martí, J., Mitjavila, J. & Araña, V. (1994). Stratigraphy, structure and geochronology of the Las Cañadas caldera (Tenerife, Canary Islands). *Geological Magazine* **131**, 715–727.
- Martí, J., Hurlimann, M., Ablay, G. J. & Gudmundsson, A. (1997). Vertical and lateral collapses on Tenerife (Canary Islands) and other volcanic ocean islands. *Geology* **25**, 879–882.
- McDonough, W. F. & Sun, S. S. (1995). The composition of the Earth. *Chemical Geology* **120**, 223–253.
- Mollo, S., Gaeta, M., Freda, C., Di Rocco, T., Misiti, V. & Scarlato, P. (2010). Carbonate assimilation in magmas: A reappraisal based on experimental petrology. *Lithos* **114**, 503–514.
- Morgan, W. J. (1983). Hotspot tracks and the early rifting of the Atlantic. *Tectonophysics* **94**, 123–139.
- Nash, W. P. & Crecraft, H. R. (1985). Partition coefficients for trace elements in silicic magmas. *Geochimica et Cosmochimica Acta* **49**, 2309–2322.
- Neumann, E. R., Sorensen, V. B., Simonsen, S. L. & Johnsen, K. (2000). Gabbroic xenoliths from La Palma, Tenerife and Lanzarote, Canary Islands: evidence for reactions between mafic alkaline Canary Islands melts and old oceanic crust. *Journal of Volcanology and Geothermal Research* **103**, 313–342.
- Nicholson, H., Condomines, M., Fitton, J. G., Fallick, A. E., Gronvold, K. & Rogers, G. (1991). Geochemical and isotopic evidence for crustal assimilation beneath Krafla, Iceland. *Journal of Petrology* **32**, 1005–1020.
- O'Hara, M. J. (1998). Volcanic plumbing and the space problem—thermal and geochemical consequences of large-scale assimilation in ocean island development. *Journal of Petrology* **39**, 1077–1089.
- Olin, P. & Wolff, J. (2010). Rare earth and high field strength element partitioning between iron-rich clinopyroxenes and felsic liquids. *Contributions to Mineralogy and Petrology* **160**, 761–775.
- Olin, P. H. & Wolff, J. A. (2012). Partitioning of rare earth and high field strength elements between titanite and phonolitic liquid. *Lithos* **128–131**, 46–54.
- Palacz, Z. A. & Wolff, J. A. (1989). Strontium, neodymium and lead isotope characteristics of the Granadilla Pumice, Tenerife: a study of the causes of strontium isotope disequilibrium in felsic pyroclastic deposits. In: Saunders, A. D. & Norry, M. J. (eds) *Magmatism in the Ocean Basins*. Geological Society, London: Special Publication **42**, 147–159.
- Paris, R., Guillou, H., Carracedo, J. C. & Torrado, F. J. P. (2005). Volcanic and morphological evolution of La Gomera (Canary Islands), based on new K–Ar ages and magnetic stratigraphy: implications for oceanic island evolution. *Journal of the Geological Society, London* **162**, 501–512.
- Pinel, V. & Jaupart, C. (2000). The effect of edifice load on magma ascent beneath a volcano. *Philosophical Transactions of the Royal Society of London* **358**, 1515–1532.
- Price, R. C., Cooper, A. F., Woodhead, J. D. & Cartwright, I. (2003). Phonolitic diatremes within the Dunedin volcano, South Island, New Zealand. *Journal of Petrology* **44**, 2053–2080.
- Rehkämper, M. & Halliday, A. N. (1998). Accuracy and long-term reproducibility of lead isotopic measurements by multiple-collector inductively coupled plasma mass spectrometry using an external method for correction of mass discrimination. *International Journal of Mass Spectrometry* **181**, 123–133.
- Reiners, P. W., Nelson, B. K. & Ghiorso, M. S. (1995). Assimilation of felsic crust by basaltic magma: Thermal limits and extents of crustal contamination of mantle-derived magmas. *Geology* **23**, 563–566.
- Ridley, W. (1970). The abundance of rock types on Tenerife, Canary Islands, and its petrogenetic significance. *Bulletin of Volcanology* **34**, 196–204.
- Rodríguez-Badiola, E., Pérez-Torrado, F. J., Carracedo, J. C. & Guillou, H. (2006). Petrografía y Geoquímica del edificio volcánico Teide–Pico Viejo y las dorsales noreste y noroeste de Tenerife. In: Carracedo, J. C. (ed.) *Los volcanes del Parque Nacional del Teide/El Teide, Pico Viejo y las dorsales activas de Tenerife*. Madrid: Organismo Autónomo Parques Nacionales Ministerio De Medio Ambiente, pp. 129–186.
- Roest, W. R., Dañobeitia, J. J., Verhoef, J. & Collette, B. J. (1992). Magnetic anomalies in the Canary Basin and the Mesozoic evolution of the Central North Atlantic. *Marine Geophysical Researches* **14**, 1–24.
- Sawyer, E. W. (1991). Disequilibrium melting and the rate of melt–residuum separation during migmatization of mafic rocks from the Grenville Front, Quebec. *Journal of Petrology* **32**, 701–738.
- Schiffman, P., Zierenberg, R., Chadwick, W. W., Jr, Clague, D. A. & Lowenstern, J. (2010). Contamination of basaltic lava by seawater: Evidence found in a lava pillar from Axial Seamount, Juan de Fuca Ridge. *Geochemistry, Geophysics, Geosystems* **11**, Q04004.
- Schmincke, H. (1969). Ignimbrite sequence on Gran Canaria. *Bulletin of Volcanology* **33**, 1199–1219.
- Schmincke, H.-U. & Rihm, R. (1994). *Ozeanvulkan 1993, Cruise No. 24, 15 April–9 May 1993*. Hamburg: University of Hamburg.
- Schmincke, H.-U., Klügel, A., Hansteen, T. H., Hoernle, K. & van den Bogaard, P. (1998). Samples from the Jurassic ocean crust beneath Gran Canaria, La Palma and Lanzarote (Canary Islands). *Earth and Planetary Science Letters* **163**, 343–360.
- Schnetzler, C. C. & Philpotts, J. A. (1970). Partition coefficients of rare-earth elements between igneous matrix material and rock-forming mineral phenocrysts—II. *Geochimica et Cosmochimica Acta* **34**, 331–340.
- Simonsen, S. L., Neumann, E. R. & Seim, K. (2000). Sr–Nd–Pb isotope and trace-element geochemistry evidence for a young HIMU source and assimilation at Tenerife (Canary Island). *Journal of Volcanology and Geothermal Research* **103**, 299–312.
- Spera, F. J. & Bohrsen, W. A. (2001). Energy-constrained open-system magmatic processes I: general model and energy-constrained assimilation and fractional crystallization (EC-AFC) formulation. *Journal of Petrology* **42**, 999–1018.
- Spera, F. J. & Bohrsen, W. A. (2002). Energy-constrained open-system magmatic processes 3. Energy-constrained recharge, assimilation, and fractional crystallization (EC-RAFC). *Geochemistry, Geophysics, Geosystems* **3**, doi:10.1029/2002GC000315.
- Spera, F. J. & Bohrsen, W. A. (2004). Open-system magma chamber evolution: an energy-constrained geochemical model incorporating the effects of concurrent eruption, recharge, variable assimilation and fractional crystallization (EC-ERA χ FC). *Journal of Petrology* **45**, 2459–2480.
- Staudigel, H. & Schmincke, H.-U. (1984). The Pliocene Seamount Series of La Palma/Canary Islands. *Journal of Geophysical Research* **89**, 11195–11215.
- Stillman, C. J., Fuster, J. M., Bennell Baker, M. J., Muñoz, M., Smewing, J. D. & Sagredo, J. (1975). Basal complex of Fuerteventura (Canary Islands) is an oceanic intrusive complex with rift-system affinities. *Nature* **257**, 469–471.

- Stronck, N., Klügel, A. & Hansteen, T. (2009). The magmatic plumbing system beneath El Hierro (Canary Islands): constraints from phenocrysts and naturally quenched basaltic glasses in submarine rocks. *Contributions to Mineralogy and Petrology* **157**, 593–607.
- Sun, S. S. (1980). Lead isotopic study of young volcanic rocks from mid-ocean ridges, ocean islands and island arcs. *Philosophical Transactions of the Royal Society of London, Series A* **297**, 409–445.
- Taylor, H. P., Jr (1980). The effects of assimilation of country rocks by magmas on $^{18}\text{O}/^{16}\text{O}$ and $^{87}\text{Sr}/^{86}\text{Sr}$ systematics in igneous rocks. *Earth and Planetary Science Letters* **47**, 243–254.
- Taylor, H. P., Jr & Sheppard, S. M. F. (1986). Igneous rocks: I. Processes of isotopic fractionation and isotope systematics. In: Valley, J. W., Taylor, H. P., Jr & O'Neil, J. R. (eds) *Stable Isotopes in High Temperature Geological Processes*. Mineralogical Society of America, *Reviews in Mineralogy* **16**, 227–272.
- Thirlwall, M. F., Jenkins, C., Vroon, P. Z. & Matthey, D. P. (1997). Crustal interaction during construction of ocean islands: Pb–Sr–Nd–O isotope geochemistry of the shield basalts of Gran Canaria, Canary Islands. *Chemical Geology* **135**, 233–262.
- Thirlwall, M. F., Singer, B. S. & Marriner, G. F. (2000). ^{39}Ar – ^{40}Ar ages and geochemistry of the basaltic shield stage of Tenerife, Canary Islands, Spain. *Journal of Volcanology and Geothermal Research* **103**, 247–297.
- Thompson, G., Smith, I. & Malpas, J. (2001). Origin of oceanic phonolites by crystal fractionation and the problem of the Daly gap: an example from Rarotonga. *Contributions to Mineralogy and Petrology* **142**, 336–346.
- Triebold, S., Kronz, A. & Wörner, G. (2006). Anorthite-calibrated backscattered electron profiles, trace elements, and growth textures in feldspars from the Teide–Pico Viejo volcanic complex (Tenerife). *Journal of Volcanology and Geothermal Research* **154**, 117–130.
- Troll, V. R. & Schmincke, H. U. (2002). Magma mixing and crustal recycling recorded in ternary feldspar from compositionally zoned peralkaline ignimbrite A, Gran Canaria, Canary Islands. *Journal of Petrology* **43**, 243–270.
- Troll, V. R., Walter, T. R. & Schmincke, H. U. (2002). Cyclic caldera collapse: Piston or piecemeal subsidence? Field and experimental evidence. *Geology* **30**, 135–138.
- Troll, V. R., Donaldson, C. H. & Emeleus, C. H. (2004). Pre-eruptive magma mixing in ash-flow deposits of the Tertiary Rum Igneous Centre, Scotland. *Contributions to Mineralogy and Petrology* **147**, 722–739.
- Troll, V. R., Chadwick, J. P., Ellam, R. M., McDonnell, S., Emeleus, C. H. & Meighan, I. G. (2005). Sr and Nd isotope evidence for successive crustal contamination of Slieve Gullion ring-dyke magmas, Co. Armagh, Ireland. *Geological Magazine* **142**, 659–668.
- Troll, V. R., Nicoll, G. R., Donaldson, C. H. & Emeleus, H. C. (2008). Dating the onset of volcanism at the Rum Igneous Centre, NW Scotland. *Journal of the Geological Society, London* **165**, 651–659.
- Verhoef, J., Collette, B. J., Dañoibeitia, J. J., Roeser, H. A. & Roest, W. R. (1991). Magnetic anomalies off West-Africa (20–38°N). *Marine Geophysical Researches* **13**, 81–103.
- Walter, T. R. & Troll, V. R. (2003). Experiments on rift zone evolution in unstable volcanic edifices. *Journal of Volcanology and Geothermal Research* **127**, 107–120.
- Walter, T. R., Troll, V. R., Cailleau, B., Belousov, A., Schmincke, H. U., Amelung, F. & van den Bogaard, P. (2005). Rift zone reorganization through flank instability in ocean island volcanoes: an example from Tenerife, Canary Islands. *Bulletin of Volcanology* **67**, 281–291.
- Watts, A. B. & Masson, D. G. (1995). A giant landslide on the north-flank of Tenerife, Canary Islands. *Journal of Geophysical Research* **100**, 24487–24498.
- Watts, K. E., Bindeman, I. N. & Schmitt, A. K. (2011). Large-volume rhyolite genesis in caldera complexes of the Snake River Plain: insights from the Kilgore Tuff of the Heise Volcanic Field, Idaho, with comparison to Yellowstone and Bruneau–Jarbridge rhyolites. *Journal of Petrology* **52**, 857–890.
- Wellman, T. R. (1970). The stability of sodalite in a synthetic syenite plus aqueous chloride fluid system. *Journal of Petrology* **11**, 49–72.
- White, W. M., Albarède, F. & Télouk, P. (2000). High-precision analysis of Pb isotope ratios by multi-collector ICP-MS. *Chemical Geology* **167**, 257–270.
- Wiesmaier, S. (2010). *Magmatic differentiation and bimodality in oceanic island settings—implications for the petrogenesis of magma in Tenerife, Spain*. Trinity College Dublin, 191 p.
- Wiesmaier, S., Deegan, F., Troll, V. R., Carracedo, J. C., Chadwick, J. P. & Chew, D. (2011). Magma mixing in the 1100 AD Montaña Reventada composite lava flow, Tenerife, Canary Islands: interaction between rift zone and central volcano plumbing systems. *Contributions to Mineralogy and Petrology* **162**, 651–669.
- Williams, L. (1970). The volcanics of the Gregory Rift Valley, east Africa. *Bulletin of Volcanology* **34**, 439–465.
- Williams, L. A. J. (1972). The Kenya Rift volcanics: A note on volumes and chemical composition. *Tectonophysics* **15**, 83–96.
- Williams, M. L., Hanmer, S., Kopf, C. & Darrach, M. (1995). Syntectonic generation and segregation of tonalitic melts from amphibolite dikes in the lower crust, Striding–Athabasca mylonite zone, northern Saskatchewan. *Journal of Geophysical Research* **100(B8)**, 15717–15734.
- Wolff, J. A. (1983). *Petrology of Quaternary pyroclastic deposits from Tenerife, Canary Islands*. University of London, 542 p.
- Wolff, J. A. (1987). Crystallisation of nepheline syenite in a subvolcanic magma system: Tenerife, Canary islands. *Lithos* **20**, 207–223.
- Wolff, J. A. & Palacz, Z. A. (1989). Lead isotope and trace element variation in Tenerife pumices—evidence for recycling within an ocean island volcano. *Mineralogical Magazine* **53**, 519–525.
- Wolff, J. A. & Storey, M. (1983). The volatile component of some pumice-forming alkaline magmas from the Azores and Canary Islands. *Contributions to Mineralogy and Petrology* **82**, 66–74.
- Wolff, J. A. & Storey, M. (1984). Zoning in highly alkaline magma bodies. *Geological Magazine* **121**, 563–575.
- Wolff, J. A., Grandy, J. S. & Larson, P. B. (2000). Interaction of mantle-derived magma with island crust? Trace element and oxygen isotope data from the Diego Hernandez Formation, Las Canadas, Tenerife. *Journal of Volcanology and Geothermal Research* **103**, 343–366.
- Wörner, G., Beusen, J. M., Duchateau, N., Gijbels, R. & Schmincke, H. U. (1983). Trace element abundances and mineral/melt distribution coefficients in phonolites from the Laacher See volcano (Germany). *Contributions to Mineralogy and Petrology* **84**, 152–173.
- Ye, S., Canales, J. P., Rihm, R., Dañoibeitia, J. J. & Gallart, J. (1999). A crustal transect through the northern and northeastern part of the volcanic edifice of Gran Canaria, Canary Islands. *Journal of Geodynamics* **28**, 3–26.